JOURNAL OF MATERIALS SCIENCE 26 (1991) 4702–4720

Effects of interfacial coating and temperature on the fracture behaviours of unidirectional Kevlar and carbon fibre reinforced epoxy resin composites

JANGKYO KIM, YIU-WING MAI
Centre for Advanced Materials Technology, Department of Mechanical Engineering, University of Sydney, Sydney, NSW 2006, Australia

The enhancement of transverse fracture toughness of unidirectional Kevlar and carbon fibre reinforced epoxy resin composites (KFRP and CFRP) has been studied using polymer coatings on the fibres. The results obtained show a substantial improvement in the impact fracture toughness of both KFRP and CFRP with polyvinyl alcohol (PVAL) coating without any loss of flexural strength; but there is only a moderate increase in impact toughness with other types of coating (i.e. carboxyl-terminated butadiene acrylonitrile (CTBN) copolymer and polyvinyl acetate (PVA)) with some reduction in flexural strength. The dependence of impact fracture toughness of these composites (with and without PVAL coating) on temperature was analysed on the basis of existing theories of toughening mechanisms from measurements of fibre–matrix interfacial properties, debond and fibre pull-out lengths and microscopic observations. The beneficial effect of fibre coating with PVAL on transverse fracture toughness is shown to sacrifice little damage tolerance of the composites against delamination fracture.

1. Introduction

Fibre composite technology is based on taking advantage of the high specific strength and stiffness of fibres by dispersing them in a resin matrix, which acts as a binder and transfers stresses to the fibres across the interface. In addition to strength and stiffness, another important property of a composite is its specific resistance to fracture or fracture toughness. It is well known that the fracture toughness of a composite is not simply the sum of the weighted contributions by the constituents, but is governed more importantly by the extent of energy absorption processes through various toughening mechanisms, depending on the nature of bonding and morphology at the fibre–matrix interface. These toughening mechanisms include interfacial debonding [1], post-debonding friction [2], stress redistribution after fibre breakage [3, 4] and fibre pull-out [5, 6], in addition to fractures of fibre and matrix. Strong bonding is essential for efficient stress transfer and thus to achieve high strength. However, this generally leads to a catastrophic failure with cracks propagating right through the matrix and fibres, and the resultant energy dissipation is therefore usually limited to the work done in creating new fracture surfaces. In contrast, weak interfacial bonding allows the said toughening mechanisms to occur more extensively during the whole fracture process, giving large contributions to the fracture toughness of the composite.

Since a critical design criterion in fibre composites is sufficient fracture energy absorption capability, particularly in impact loading situations, there have been a number of attempts to improve the composite fracture toughness without significant loss of tensile or flexural strength. These can be generally classified into two approaches: one relies on the improvement of the intrinsic properties of composite constituents and the other depends on suitable interface controls. The first approach includes the use of tough matrix materials (e.g. rubber-toughened epoxies and thermoplastics) and fibre hybrids (e.g. mixture of Kevlar, glass and carbon fibres). The second approach includes fibre coatings with appropriate polymers, non-fracturing duplex fibres, delamination arresters and promoters, reduction of shrinkage stresses in the matrix, etc. A comprehensive review on these toughening methods and the various factors which would affect the efficiency of enhancement of toughness is given recently by Kim and Mai [7].

One of the most effective methods in controlling the interface to enhance the fracture toughness of fibre composites is the application of polymer coatings, either fully or intermittently along the fibre length. Because of the simplicity in application to practical composites and the feasibility of direct comparison of fracture behaviours between the composites with and without coating, the fibre coating technique has received most attention from researchers amongst various toughening methods. The principal effect of altering the interfacial properties by fibre coating is to modify the mode of failure and thus the potential energy absorption capacity, which in turn determines

0022–2461/91 $03.00 + .12

the fracture toughness of the composite [8]. Harris and Beaumont [9, 10] found that carbon fibres coated with a silicon fluid resulted in the fibres being surrounded by an inert film which reduced the interfacial bond strength (τ_b) and thus increased the toughness of carbon fibre reinforced plastics (CFRP). In a similar study on CFRP with silicon rubber-coated fibres, Hancox and Wells [11] were able to improve the toughness of CFRP by some 100% at the expense of up to 60% loss of flexural strength, depending on the coating thickness. Since the main source of the fracture toughness of most high-performance fibre composites is by fibre pull-out, it would be necessary to maintain sufficiently high frictional shear stress (τ_f), in addition to weakening τ_b, so that the work of fibre pull-out could be enhanced. The frictional fibre pull-out work was investigated by Sung *et al.* [12], where the reinforcing fibres were coated with a thin layer of strain-rate sensitive viscous fluid, e.g. silicon vacuum fluid (SVF). They proposed that at a given strain rate the viscous shear stress acting on the fibres during pull-out and consequently the fibre pull-out toughness could be maximized by selecting coatings of high fluid viscosity and small thickness. Other investigators have successfully applied different types of polymer coating to different composites: polysulphone, polybutadiene on CFRP [11, 13]; latex coatings (e.g. polybutyl acrylate, polyethyl acrylate, etc.) on glass fibre–epoxy resin composites (GFRP) [14, 15]; anhydride copolymers (e.g. polybutadiene–co-maleic anhydride (BMA) and polymethylvinylether–co-maleic anhydride) [16, 17] and acrylonitrile copolymers (e.g. acrylonitrile–methylacrylate and acrylonitrile–glycidylacrylate) on CFRP [18–20]. In particular, Peiffer and Nielsen [14, 15] had achieved a significant 600% increase in the impact toughness of GFRP with negligible strength reduction, using colloidal latex particles which were attracted to glass fibres by electrostatic forces to form a rubbery acrylic layer of uniform thickness. They proposed that the impact toughness was a function of both thickness and glass transition temperature (T_g) of the coating: the toughness was a maximum when the coating had a low T_g and a thickness about 0.2 μm.

Although the intermittent bonding method utilizes the same fibre coating technique, its proposed toughening mechanisms are peculiar and different from the energy-absorbing mechanisms which can be obtained from full fibre coating. Marston *et al.* [21, 22] proposed that provided there were enough regions of strong interfacial bond to ensure the high composite strength, the rest of the composite could have quite a weak bond which would serve to blunt the running crack by the Cook–Gordon mechanism [23]. If a composite is laid up randomly with respect to weak and strong regions, both high strength and high toughness should be simultaneously obtained. Atkins [22, 24] increased the fracture toughness of boron fibre–epoxy resin composites (BFRP) using an 80% coating of polyurethane varnish (PUV) by 400% with less than 10% loss of tensile strength, while the improvement in toughness with silicon vacuum grease (SVG) was only 10 to 15%, even though τ_b values of the fibres coated with the two coating materials were similar. This indicates that a similar τ_b may not necessarily mean a similar fracture toughness. Atkins attributed this to the Cook–Gordon debonding mechanism that took place with the PUV coating which increased the fibre pull-out length, whereas this mechanism was non-existent with the SVG coating. Atkins and Mai [25] confirmed that the intermittently bonded composites could be favourably used in adverse environmental conditions such as hygrothermal ageing. Later, Mai and coworkers [26–29] performed extensive studies with Kevlar fibre reinforced plastics (KFRP) using SVF and a blend of polyester–polyether resins (Estapol). They investigated the effects of hygrothermal ageing, percentage coating over a repeated fibre length, fatigue damage, strain rate and temperature on the tensile strength, modulus and fracture toughness of the composites. They showed that the fracture toughness of Estapol-coated composites could be increased by some 200 to 300%, particularly at high temperatures and low strain rates, without introducing any significant reduction in tensile strength.

In the present study, as part of a larger project on the development of high-strength and high-toughness composites with controlled interfaces, several organic polymers were employed as coatings on fibres and their effects on the interfacial properties and fracture toughness in the transverse direction were studied for KFRP and CFRP. Initially, unidirectional fibre composite laminates were used for toughness measurements on a Charpy impact tester. Impact testing has long been one of the most useful and popular industrial tools to evaluate, at least in a comparative sense when standardized specimen geometry is used, the energy absorption capability of engineering materials with minimum complications of specimen preparation and testing. However, it was realized that the measured value of impact energy might not be a material property but was rather a function of specimen dimensions and other testing variables, as pointed out by many previous investigators [30–34].

For KFRP, a significant part of the specimen depth was not broken but was forced through the gap between the anvils, causing plastic bending in the back-face of the specimen. This observation held even at low test temperatures, and was more pronounced for large fibre volume fractions (V_f) and for fibres with a polymer coating. This was attributed mainly to the ductile nature of the Kevlar fibres, which was manifested in static bending where the load did not diminish to zero even at a deflection several times greater than the specimen depth. Poor machinability of the KFRP [35] was another problem encountered in cutting specimens to the required geometries for testing. For CFRP, although specimens were broken completely into halves after impact, a transition of failure mode was evident across the specimen depth. Examination of the fracture surface showed a ragged appearance with pulled-out fibre bundles in the tension side and a smooth plane without fibre pull-out in the area subjected to compression. There was always a

distinct line between these two fracture surfaces near the neutral axis of bending. This problem made it difficult to evaluate the inherent fracture energy absorption of the fibre composites because it would depend strongly on the specimen depth. Also, it was difficult to measure, with any accuracy, the debond and fibre pull-out lengths from the fracture surfaces (which are required to determine the toughness results) when composites of large V_f were involved.

Therefore, in the subsequent study, these difficulties were overcome by employing sandwich specimens fabricated from monolayer composites and epoxy resin. This method had been successfully employed in the study of fracture toughness of ductile polymers by sandwiching thin layers of epoxy resin to promote brittle cracking [36]. Other investigators [37, 38] also used a similar technique for glass–carbon hybrid fibre composites where one layer of fibre bundles was placed near the tension face to ensure all the fibres would fail under tension in static three-point flexure. The direction of loading was across the laminar plane and was different from that of the present work. The effect of temperature on impact fracture toughness in the range between -50 and $+80\,^{\circ}C$ was studied for KFRP and CFRP.

Although the toughening methods described earlier are effective for enhancing the transverse fracture toughness, the introduction of deliberately weakened fibre–matrix and/or laminar interfaces, particularly in methods using fibre coatings and delamination promoters, may produce excessive interfacial debonding and delamination which would cause unacceptable reductions in stiffness and other mechanical properties of the composite. The high degree of anisotropy and laminar structures of most fibre composite components imply that inter-ply delamination is one of the most prevalent life-limiting damage modes in this kind of material. Therefore, the delamination behaviours of these fibre composites were also characterized in mixed mode I–II delamination fracture.

2. Experimental procedure

2.1. Materials and fabrication of unidirectional fibre composites and sandwiches

The fibres used were an aramid fibre, Kevlar 49 (E.I. du Pont de Nemours Co. Inc., USA) and a carbon fibre grade HTA (Aerotex, USA) both in the form of continuous roving. The matrix material was an epoxy resin, Araldite GY260 (Ciba Geigy, Australia), a diglycidal ether of bisphenol A (DGEBA), and curing agent piperidine in the ratio of 100:5 by weight. The coating materials were selected on the basis of their mechanical properties and compatibility with the fibres. In this study three polymer coatings were employed: carboxyl-terminated butadiene acrylonitrile (CTBN) copolymer, polyvinyl acetate (PVA) and polyvinyl alcohol (PVAL). The CTBN was diluted with acetone, and PVA and PVAL were dissolved in distilled water. The fibres, while being maintained straight using clamps, were immersed in a coating solution and then subsequently dried at room temperature for at least 4 h. The amount of coating was controlled by the concentration of the coating solution. Unidirectional composites were made by hand lay-up and vacuum bagging on a steel mould, and were cured in an autoclave for 16 h at 120 °C. Vacuum pressure of -100 kPa was applied for the initial 30 min to enable evaporation of entrapped air bubbles, followed by compressive pressure of 200 kPa for the rest of the cure cycle. Composites with a uniform V_f of approximately 50% and final thickness 4.0 $\pm$ 0.24 mm could be produced by employing equal amounts of resin and an equal number of bleeders for each mould, as determined in preliminary tests.

For the reasons described in Section 1, monolayer composites sandwiched by epoxy resin layers were used for the study of temperature effects on the fracture toughness of uncoated and PVAL-coated fibre composites. Having fabricated the monolayer composites by the foregoing procedure, sandwich panels were produced on a split-frame mould where the composite monolayer was placed at a desired position (i.e. in the mid-plane for impact test specimens and 1.5 mm apart from one surface for delamination test specimens), using slotted non-stick Teflon dams and epoxy resin filling in the cavity (Fig. 1). The epoxy resin and the curing procedures employed were the same as for the composite laminates. To separate the

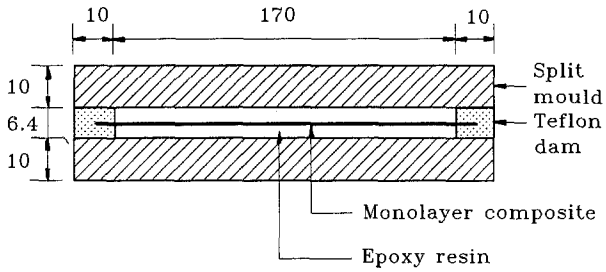

Figure 1 Split frame mould for fabrication of monolayer composite–epoxy resin sandwiches (dimensions in mm).

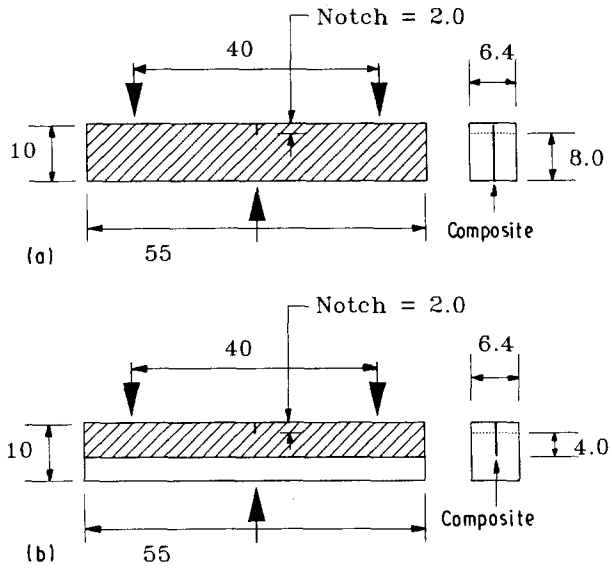

Figure 2 Sandwich specimens in Charpy impact tests: (a) full ligament with monolayer composite; (b) monolayer composite in tension side (dimensions in mm).

toughness contribution due to fracture of the composite ligament in the compression side, cut-size composite monolayers were also used for the sandwich specimens with the monolayer placed only in the tension side (Fig. 2b). The total thickness of the sandwich was 6.4 ± 0.1 mm and the average thickness of composite monolayers without and with PVAL coating were 0.20 and 0.21 mm for KFRP and 0.54 and 0.56 mm for CFRP, respectively.

2.2. Specimens and tests

2.2.1. Charpy impact tests

The fracture toughness of composites was evaluated using a Zwick Charpy impact tester of total span 40 mm and full scale 4 J at an impact velocity 2.93 m s^{-1}. For sandwich specimens the full scale was reduced to 2 J because of the low impact energy dissipated by the fractured specimen. Specimens 10 mm wide and 55 mm long were cut from the composite laminates and sandwich panels. Notches were made in the width direction of the centre span using a circular saw 0.8 mm thick and the notch tip was further sharpened by tapping with a scalpel blade. For KFRP laminates, the specimen width was reduced to 6 mm to suit the maximum capacity of the impact tester and the notch tip was sharpened using a saw of thickness 0.5 mm, because tapping a scalpel blade did not produce a satisfactory result.

For the composite laminate specimens, fracture toughness was determined directly from the impact energy (U) absorbed divided by the specimen ligament area (A). For the sandwich specimens (Fig. 2a and b), the fracture toughness of composites (R_c) was calculated from the known dimensions of each layer and the fracture toughness of the epoxy layer (R_e) on the basis of the Rule of Mixtures [36]: i.e.

$$U = R_s A_s = R_c A_c + R_e A_e \quad (1)$$

$$R_c = \frac{U - R_e A_e}{A_c} \quad (2)$$

Subscripts s, c and e refer to the sandwich, composite and epoxy layers, respectively. To investigate the effect of temperature on fracture toughness, tests were conducted in the temperature range − 50 to + 80 °C which covered the extremes of the thermal performance range of polymer-matrix composite structures [39]. Temperature control was achieved in an air-circulated Instron environmental chamber. When the desired temperature was reached specimens were put inside the chamber and left to reach equilibrium. Specimens for tests at low temperatures were shielded in a plastic bag to avoid direct contact with liquid nitrogen. The temperature drop of the specimen which might occur during transportation from the temperature chamber to the impact tester was also allowed for by using a predetermined calibration chart.

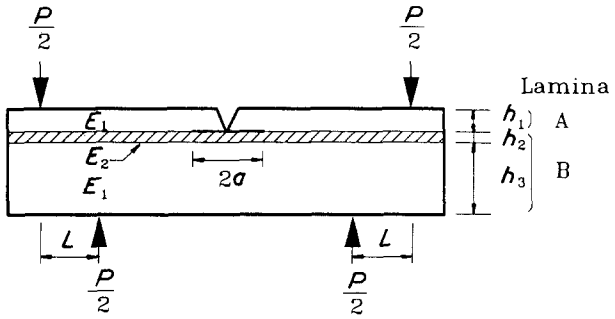

Figure 3 A monolayer composite–epoxy resin sandwich specimen in a delamination fracture test under four-point bending (width = b).

2.2.2. Mixed mode I–II delamination fracture tests

The specimen employed for the delamination fracture tests (Fig. 3) was a tri-layer beam subjected to four-point flexure where a monolayer composite (of thickness h_2) was sandwiched by identical epoxy resin layers with different thicknesses (h_1 and h_3). By regarding the specimen with an initial symmetrical crack $2a$ along the interface between laminae A and B as a bi-layer beam, an energy balance theory similar to that proposed by Kendall [40] was used to provide a criterion for crack propagation along the interface under constant bending moment. The specimen geometry provided a mixed mode I–mode II loading [41] although the mode II component was dominant. By considering the energy changes as the crack moves a distance da, the specific work of fracture (G_{I-II}) in mixed mode delamination was given by [42]

$$G_{I-II} = \frac{M^2 + 2Ma(dM/da)}{2b}\left(\frac{1}{E_2 I_B} - \frac{1}{E_1 I_S}\right) \quad (3)$$

M ($= PL/2$) is the bending moment, with P being the total bending force (for a given width b) and L ($= 10$ mm) the spacing between the inner and outer loading points. E is elastic modulus and I moment of inertia; subscripts B and S refer to lamina B and the sandwich, respectively. I_B and I_S can be calculated according to the Euler–Bernoulli elastic beam theory:

$$I_B = b\left(\frac{h_2^3}{12} + \frac{h_3^3}{12\beta} + \frac{h_2 h_3 (h_2 + h_3)^2}{4\beta[h_2 + (h_3/\beta)]}\right) \quad (4)$$

and

$$I_S = b\left(\frac{h_1^3}{12} + \frac{\beta h_2^3}{12} + \frac{h_3^3}{12} + \frac{h_1 h_3 (h_1 + 2h_2 + h_3)^2 + \beta h_2 [h_1 (h_1 + h_2)^2 + h_3 (h_2 + h_3)^2]}{4(h_1 + \beta h_2 + h_3)}\right) \quad (5)$$

where β is the ratio of elastic moduli E_2/E_1. Details of test procedures and the calculation of G_{I-II} were given elsewhere [42].

2.2.3. Other tests and microscopy

The flexural strength and interlaminar shear strength (ILSS) of composites were determined in three-point flexure of unnotched composite laminate specimens with the span-to-depth ratios of 30:1 and 5:1, respectively. Single-filament pull-out tests were performed to

TABLE I Impact fracture toughness and flexural properties of fibre composites (mean value ± standard deviation)

Composite	Coating	Coating solution concentration (%)	Impact fracture toughness ($kJ\,m^{-2}$)	Flexural strength (MPa)	Interlaminar shear strength (MPa)
Kevlar 49–epoxy	Uncoated	0	154	518 ± 38	42.6 ± 2.8
	CTBN	3.0	180	502 ± 43	43.6 ± 4.1
		6.0	167	464 ± 29	42.5 ± 3.8
		10	154	412 ± 21	40.6 ± 2.9
	PVA	2.0	168	512 ± 28	30.9 ± 3.3
		4.0	190	462 ± 31	26.6 ± 2.4
		6.0	146	386 ± 16	20.9 ± 3.1
	PVAL	4.0	260	522 ± 47	25.4 ± 1.7
Carbon–epoxy	Uncoated	0	104	683 ± 38	58.9 ± 2.3
	PVAL	4.0	144	758 ± 47	50.0 ± 3.3

evaluate the interfacial properties of uncoated and PVAL-coated Kevlar fibres. Tensile tests of Kevlar fibres and pure epoxy resins were also performed at varying temperatures. All flexure, fibre pull-out and tensile tests were conducted on an Instron testing machine with a crosshead speed of 0.5 mm min^{-1}.

The mean debonded length ($\bar{l}_d$) and maximum fibre pull-out length (l_{po}) were determined on each impact-tested sandwich specimen, using an optical profilometer with a magnifying (×10) projector and both reflected and transmitted light in a manner similar to that described by others [37, 38]. The fracture surfaces of both impact and delamination test specimens were examined with an optical stereomicroscope and a scanning electron microscope (SEM). The surface morphologies of uncoated and coated fibres were also characterized using an SEM.

3. Results

3.1. Fracture toughness of composite laminate specimens

Impact fracture toughness values for KFRP without interfacial coating are compared with those having polymer coatings on the fibres as a function of ligament length (i.e. total specimen depth minus the notch depth, $(D - a)$) in Fig. 4. The results for CFRP are shown in Fig. 5. The flexural strength and ILSS of uncoated and coated specimens with varying coating concentrations are given in Table I. Also included are the maximum impact toughness values taken from Figs 4 and 5 for equal ligament lengths of about 3.5 and 7.0 mm for KFRP and CFRP, respectively. The fracture toughness generally increased as the ligament length increased, whether fibres were coated or not for both composites. The CTBN and PVA coatings did not improve the fracture toughness very much, the maximum increase being about 20% for an optimum coating concentration. Furthermore, this small increase is accompanied by substantial reductions in flexural properties and ILSS, particularly for the composites with PVA-coated fibres. In contrast, PVAL coating is effective for improving the fracture toughness of both KFRP and CFRP, the improvement being respectively by about 80 and 40% at a large ligament length, without sacrificing flexural strength. In fact, for CFRP, the flexural strength is slightly improved with the PVAL coating.

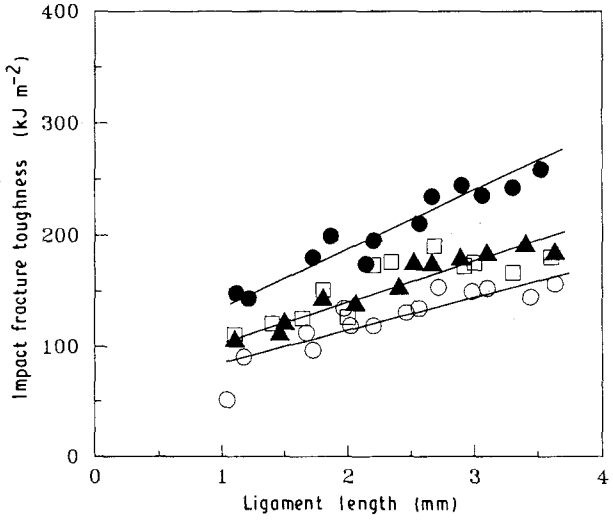

Figure 4 Impact fracture toughness of KFRP as a function of ligament length: (●) PVAL-coated (4%); (□) CTBN-coated (3%); (▲) PVA-coated (4%); (○) uncoated fibres.

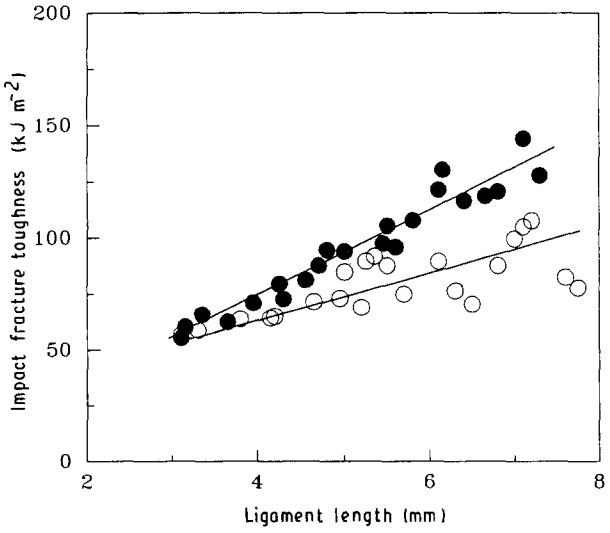

Figure 5 Impact fracture toughness of CFRP as a function of ligament length: (●) PVAL-coated (4%); (○) uncoated fibres.

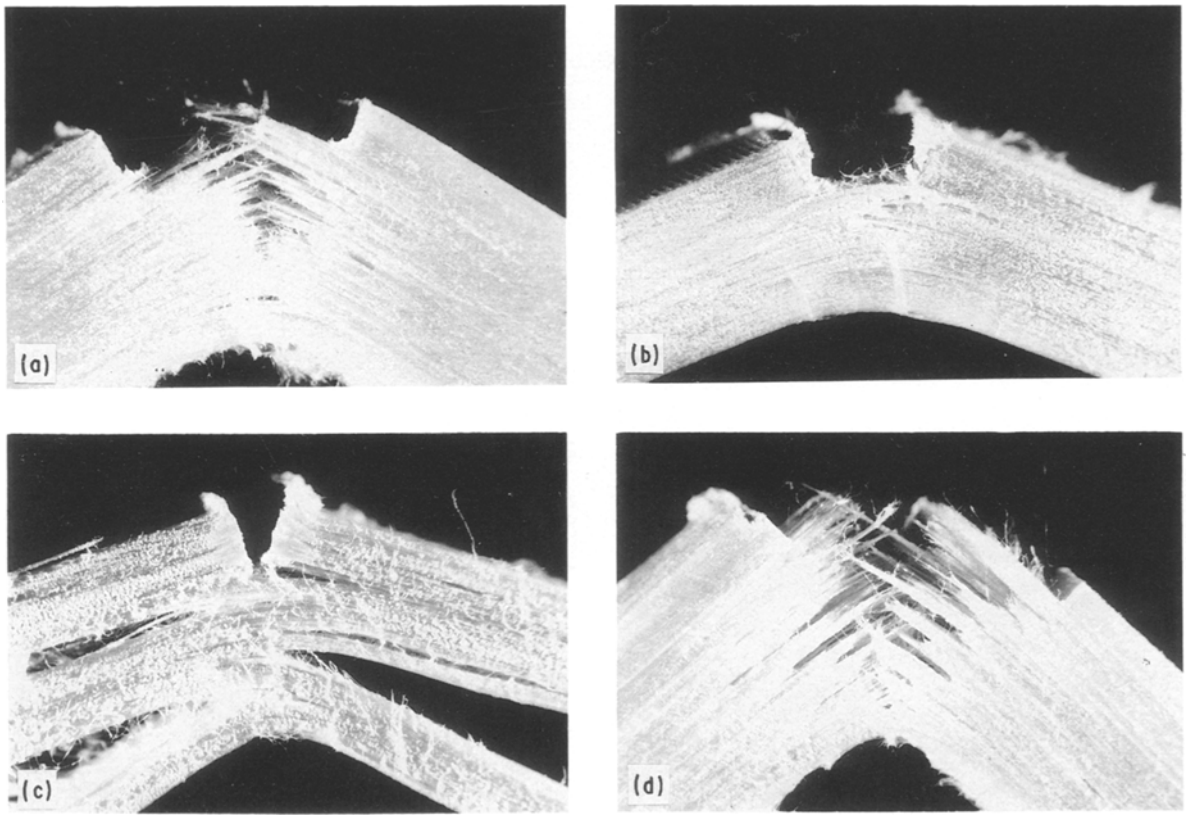

Figure 6 Photographs of typical impact KFRP specimens: (a) uncoated fibres; (b) CTBN-coated fibres; (c) PVA-coated fibres; (d) PVAL-coated fibres. (Magnification $\approx \times 5$).

Photographs of typical impact specimens for KFRP with interfacial coating are given in Fig. 6. It is found that a significant part of the ligament is not broken but is bent plastically in the compressive face, depending on the coating applied. More discussion of the fractography and its correlation with the fracture toughness of KFRP will be given in the next section.

For CFRP, although the specimens are broken completely after impact, there is an obvious change in the failure mode across the ligament: a distinct line separates the ragged and smooth fracture surfaces (which correspond to areas subjected to tension and compression, respectively, during impact fracture) as shown in Fig. 7. A similar observation has been reported recently in static flexure of CFRP [43]. The ragged surface consists of pulled-out fibre bundles, the number of fibres in a bundle ranging from several to a few hundreds, and bundling is more pronounced for uncoated CFRP. Although it is difficult to quantify the fibre pull-out lengths from the fracture surface, it is noted that increasing the ligament length slightly increases the raggedness (compare Fig. 7a and b). This observation indicates that a large ligament promotes shear failure (i.e. debonding and/or delamination) in the tension side of the specimen. The fact that the area in tension is always larger than that in compression regardless of the coating suggests that failure is always initiated from the tensile face [43, 44]. This contradicts the earlier finding [45–47] of failure initiation by compressive buckling in static flexure or impact for CFRP.

Fracture surfaces in the tension side for both uncoated and PVAL-coated CFRP are generally similar, but a distinguishable feature can be revealed on the compression side: there is extensive fibre–matrix interfacial debonding for PVAL-coated composites while this is absent for uncoated composites (compare Fig. 7c and d). The broken carbon fibres in the compression side always have one or more creases across the diameter of the fibre, their common direction perpendicular to that of loading or crack propagation and the crease separates two distinct areas of compressive and tensile failure on individual fibres. This feature is typical of fibre failure by microbuckling under compressive load for unidirectional CFRP, and the crease of individual fibres coincides with the buckling axis [43]. More importantly, the localized debonding near the compressive failure area (Fig. 7d) indicates that the fibres fail in the "shear" mode (as opposed to the "transverse" mode) where adjacent fibres buckle with the same wavelength and in phase with one another, so that the matrix material between adjacent fibres deforms primarily in shear. This is partly confirmed by some plastic shear of the matrix near the tension failure area for uncoated CFRP (Fig. 7c). The debonding in PVAL-coated composites is a direct result of low interfacial bond strength compared to the matrix shear strength, and appears to have initiated prior to compressive failure of the fibre. The debond length seems to be a function of the half-wavelength of buckling which is inversely proportional to the shear strength of the composite, as proposed in a study of a non-linear microbuckling model [48].

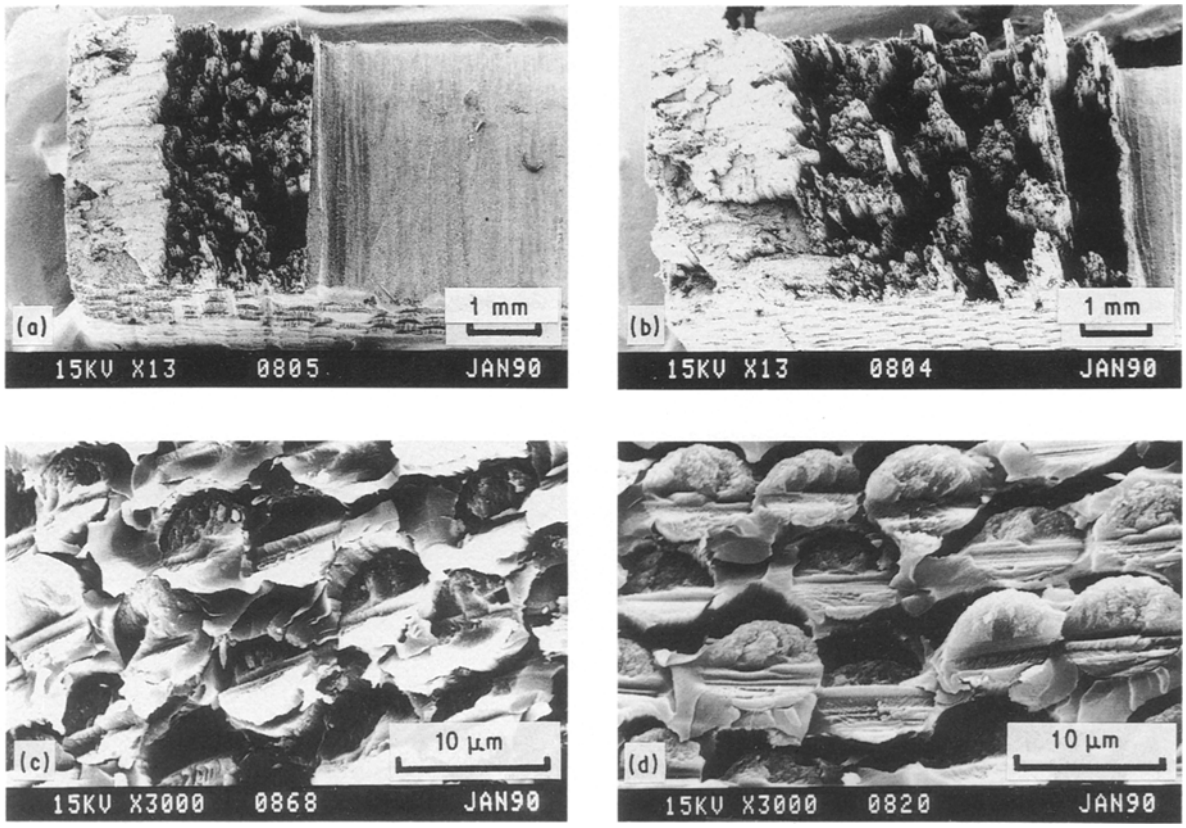

Figure 7 Fracture surfaces of CFRP impact specimens: (a) small ligament for PVAL-coated fibres; (b) large ligament for PVAL-coated fibres; (c) compression side for uncoated fibres; (d) compression side for PVAL-coated fibres.

3.2. Fracture toughness of sandwich specimens

Having succeeded in improving the fracture toughness of KFRP and CFRP with PVAL coatings on the fibres, its temperature effect was studied using monolayer composite sandwich specimens. Results from tensile tests of Kevlar 49 fibres and pure epoxy resin at different temperatures are presented in Table II. In general, as the temperature is increased, the tensile strength of both the fibre and epoxy resin decreases but the failure strain increases.

3.2.1. KFRP

Impact fracture toughness values of monolayer composites with and without PVAL coating are shown for

TABLE II Variation of mechanical properties of fibres and epoxy matrix with temperature (mean value ± standard deviation)

Material	Property	Temperature (°C)					
		− 50	− 30	0	23	50	80
Kevlar 49 fibre	Tensile strength, σ_f (MPa)	2917 ± 130	2947 ± 178	2606 ± 147	2452 ± 93	2153 ± 133	2297 ± 70
	Tensile strain, ε_f (%)	1.71 ± 0.52	2.49 ± 0.08	2.53 ± 0.47	2.87 ± 0.36	2.55 ± 0.38	2.37 ± 0.13
Carbon fibre	Tensile strength, σ_f (MPa)	–	–	–	3230*	–	–
	Tensile strain, ε_f (%)	–	–	–	1.3*	–	–
Epoxy matrix	Tensile strength, σ_m (MPa)	87.9 ± 14.0	81.5 ± 9.4	78.5 ± 0.9	66.5 ± 2.1	49.4 ± 3.5	19.4 ± 1.9
	Tensile strain, ε_m (%)	2.67 ± 0.79	2.57 ± 0.17	4.22 ± 0.12	5.22 ± 0.2	8.03 ± 3.17	30.0 ± 1.51
	Impact fracture toughness, R_c (kJ m^{-2})	1.12 ± 0.11	1.16 ± 0.01	1.15 ± 0.09	1.29 ± 0.13	1.00 ± 0.03	0.96 ± 0.10

* Manufacturer's specification.

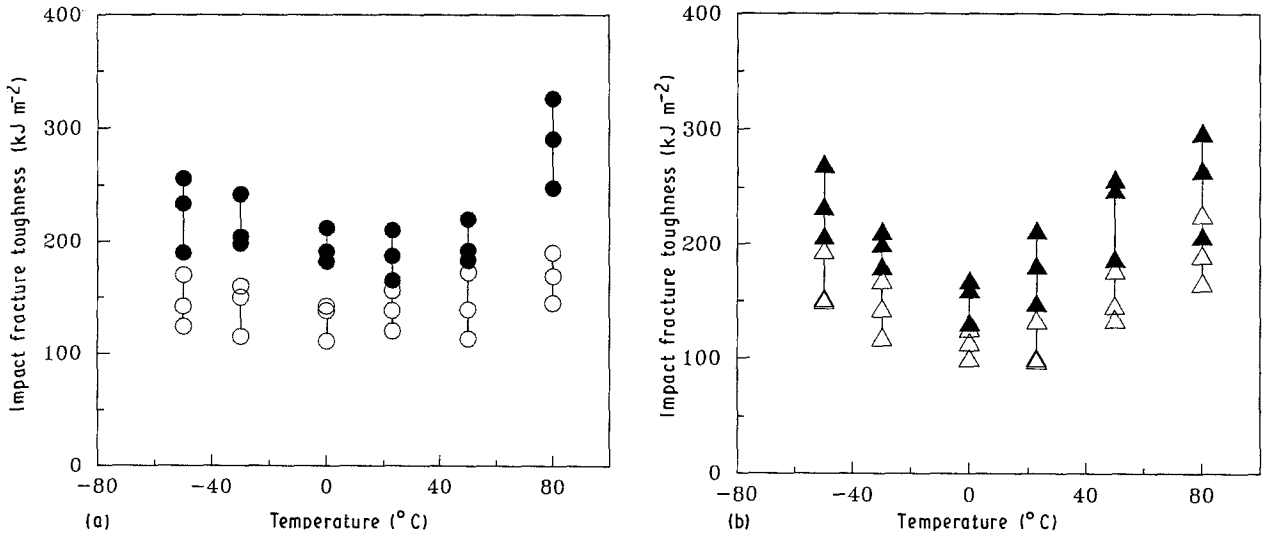

Figure 8 Variation of impact fracture toughness with temperature for KFRP: (a) full ligament with composite layer; (b) composite layer in tension side. (●, ▲) PVAL-coated; (○, △) uncoated fibres.

sandwiches with a composite layer in the full ligament and in the tension side only in Fig. 8a and b, respectively. The improvement of fracture toughness due to the PVAL coating ranges from 30 to 100% depending on the test temperature. The fracture toughness for both uncoated and coated composites shows a minimum approximately between 0 and 23 °C and a parabolic increase as the temperature further decreases or increases. A similar functional dependence of debond length ($\bar{l}_d$) on temperature can be noted in Fig. 9. However, the maximum fibre pull-out lengths (l_{po}) are almost constant and independent of temperature except at − 30 to − 50 °C for the coated specimens (Fig. 10). $\bar{l}_d$ for the sandwich specimens with composite layers in the full ligament are larger than those with composite layers placed only in the tension side (Fig. 9). In the former case, stresses at the tips of transverse cracks which propagate parallel to the fibres in the tension side are likely to be high enough to cause further debonding before the crack reaches the back face of the specimen. However, there are no significant differences in fracture toughness and l_{po} between these two types of specimen.

Typical fracture surfaces of these uncoated and PVAL-coated KFRP specimens are shown in Fig. 11, from which differences in fracture behaviour can be identified. The fibre pull-out length is significantly smaller for the former (Fig. 11a) than for the latter (Fig. 11c). Splitting of fibres into small fibrils in the longitudinal direction (i.e. fibrillation) is another important feature of uncoated KFRP (Fig. 11b). In contrast, PVAL-coated fibres tend to debond completely from the matrix with little fibrillation (Fig. 11d). It is generally observed that there is no systematic

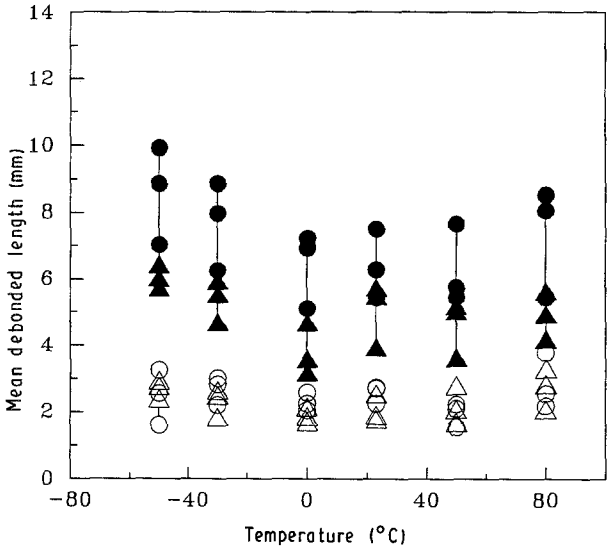

Figure 9 Variation of mean debonded length ($\bar{l}_d$) with temperature for KFRP. Full ligament with composite layer: (●) PVAL-coated; (○) uncoated. Composite layer in tension side: (▲) PVAL-coated; (△) uncoated.

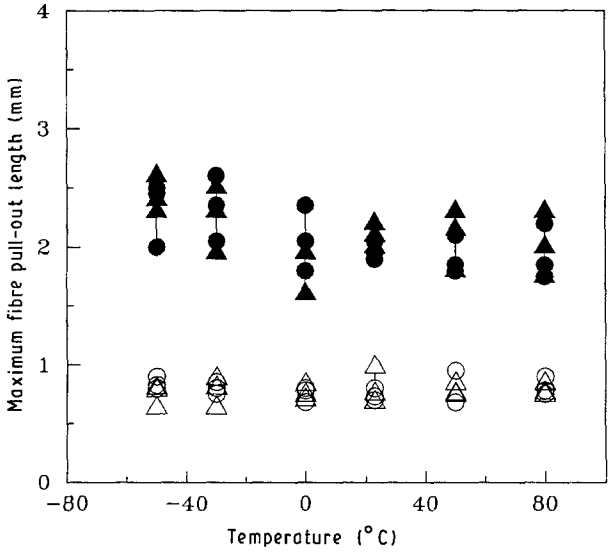

Figure 10 Variation of maximum fibre pull-out length (l_{po}) with temperature for KFRP. Full ligament with composite layer: (●) PVAL-coated; (○) uncoated. Composite layer in tension side: (▲) PVAL-coated; (△) uncoated.

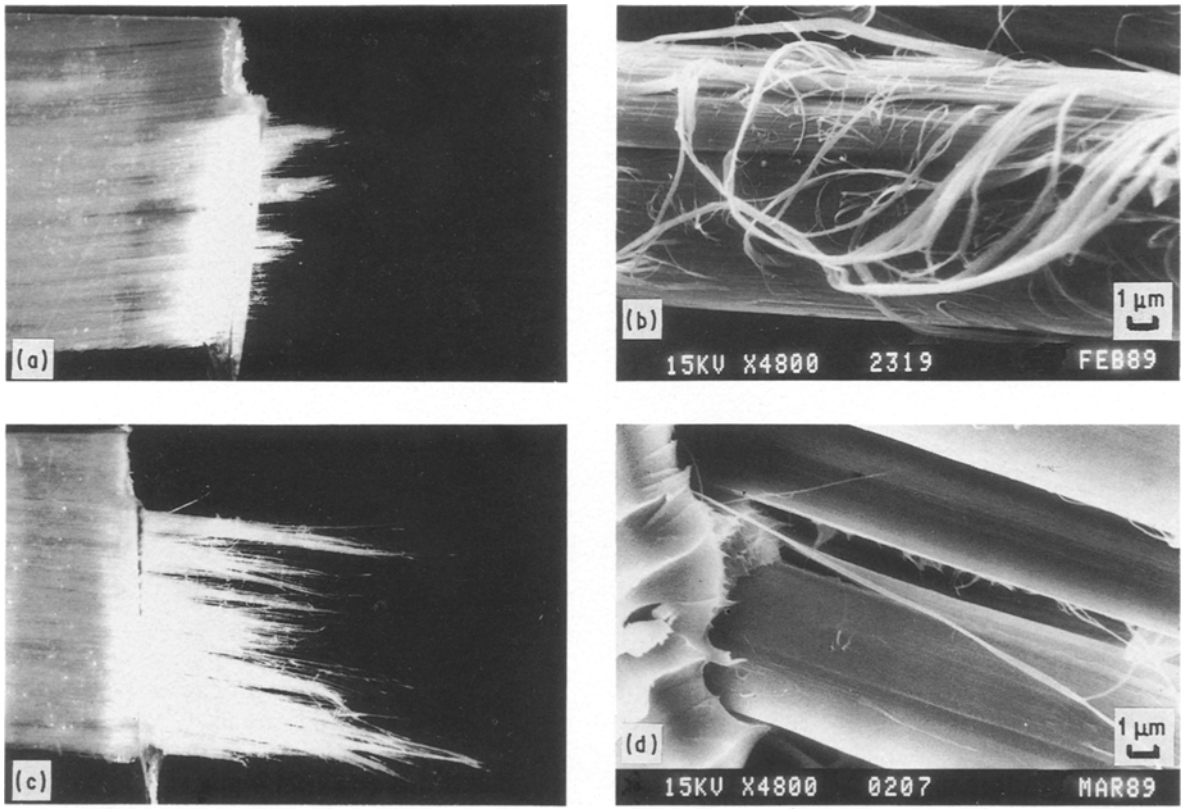

Figure 11 (a, c) Optical stereomicroscope and (b, d) SEM photographs of impact fracture surfaces for KFRP at room temperature: (a, b) uncoated fibres; (c, d) PVAL-coated fibres. (Magnifications for (a) and (c) = ×7).

variation in l_{po} across the ligament, and almost all the ligament appears to have been fractured by the crack propagated from the notch in the tension side.

Fibre debond stress (at the maximum pull-out force) and fibre pull-out stress after debonding (where frictional pull-out initiates), measured from single-filament pull-out tests for the Kevlar–epoxy system, are plotted against embedded length of fibre in Fig. 12a and b, respectively. The average bond strength (τ_b) and average frictional shear stress (τ_f) for the uncoated and PVAL-coated fibres are determined from the slopes of the lines in the respective figures. The upper-bound fibre debond stress (σ_d) is also obtained from the plateau value in Fig. 12a, where the debond stress is approximately constant and independent of the embedded length [49]. It is noted that τ_b for uncoated Kevlar fibres (45.8 MPa) is in good agreement with the ILSS (42.6 MPa in Table I) for the same composite system.

3.2.2. CFRP

The impact fracture toughness of PVAL-coated CFRP is improved by about 100% over that of the uncoated counterpart, particularly at the low-temperature end, as shown in Fig. 13. The fracture toughness

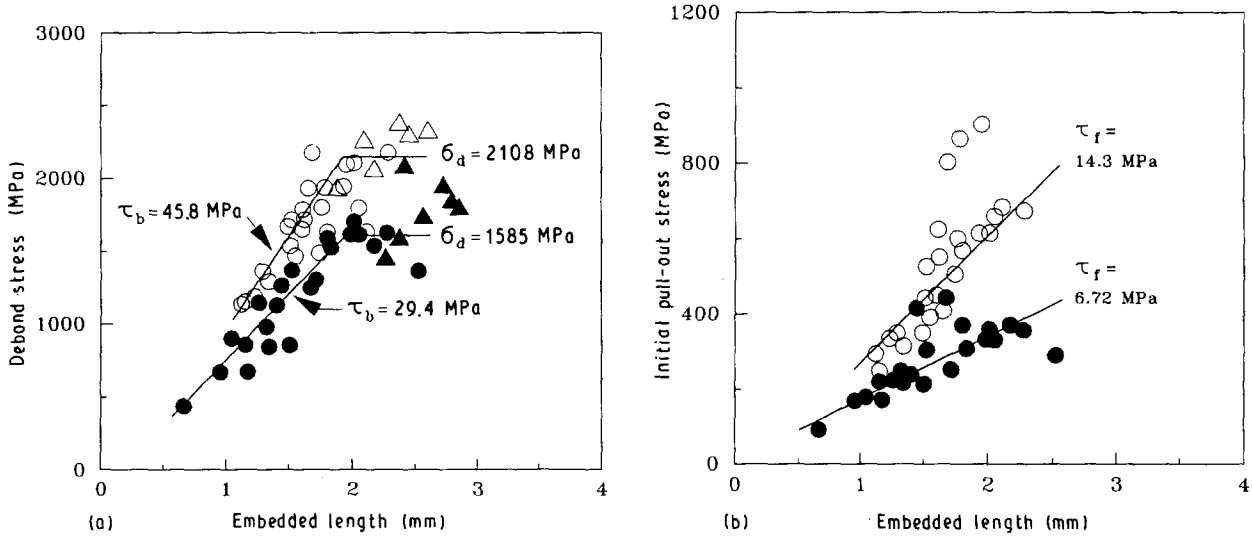

Figure 12 (a) Fibre debond stress and (b) frictional pull-out stress as a function of fibre embedded length for KFRP: (●) PVAL-coated; (○) uncoated; (▲, △) broken fibres.

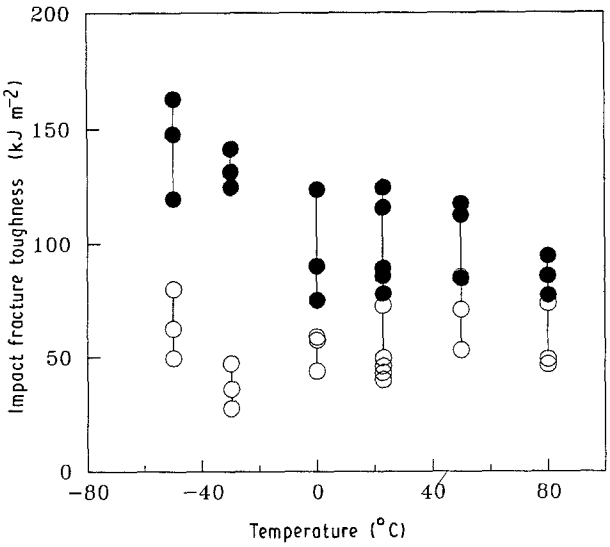

Figure 13 Variation of impact fracture toughness with temperature for CFRP: (●) PVAL-coated; (○) uncoated fibres.

of the uncoated composites increases with increasing temperature except at − 50 °C; however, the fracture toughness of the coated composites varies approximately inversely with temperature. There is a similar dependence of l_{po} on temperature as shown in Fig. 14a. Also, from the plot of the fracture toughness against l_{po} shown in Fig. 14b it is noted that the impact fracture toughness is approximately linearly dependent on l_{po} for both uncoated and PVAL-coated fibre composites. This indicates that fibre pull-out is a dominant source of fracture toughness of CFRP [10, 37, 38] regardless of the interfacial coating. The slope of the lines encompassing the data points in Fig. 14b is a direct function of the interfacial friction stress (τ_f) or fibre tensile strength (σ_f). Further, extrapolation of these lines to zero l_{po} yields approximately 10 to 45 kJ m^{-2}, which represents the sum of the remaining toughness due to other failure mechanisms. Values of $\bar{l}_d$ for CFRP (Fig. 15) are significantly smaller than for KFRP (Fig. 9), particularly for uncoated fibres, suggesting that the relatively small toughness contributions are due to fibre debonding and post-debonding friction.

Distinguishable features are revealed from the SEM photomicrographs for the uncoated and PVAL coated specimens shown in Fig. 16. One of the main characteristics of uncoated specimens is a short fibre bundle pull-out with intact matrix binding the fibres (Fig. 16a), which is a direct result of bundle debonding. The debonding of single fibres seldom occurs because the debond stress is greater than the fibre strength for carbon–epoxy composites with strong interfacial bond strength and high-stiffness fibres [50]. In contrast, PVAL-coated specimens show a combination of long individual fibres and fibre bundle pull-out (Fig. 16c), the former being more pronounced at low temperatures where high toughness values are obtained. This suggests that the relatively low interfacial bond strength with PVAL-coated fibres promotes the debonding and pull-out of individual fibres, which is partly responsible for the high toughness. Hackle markings observed in the

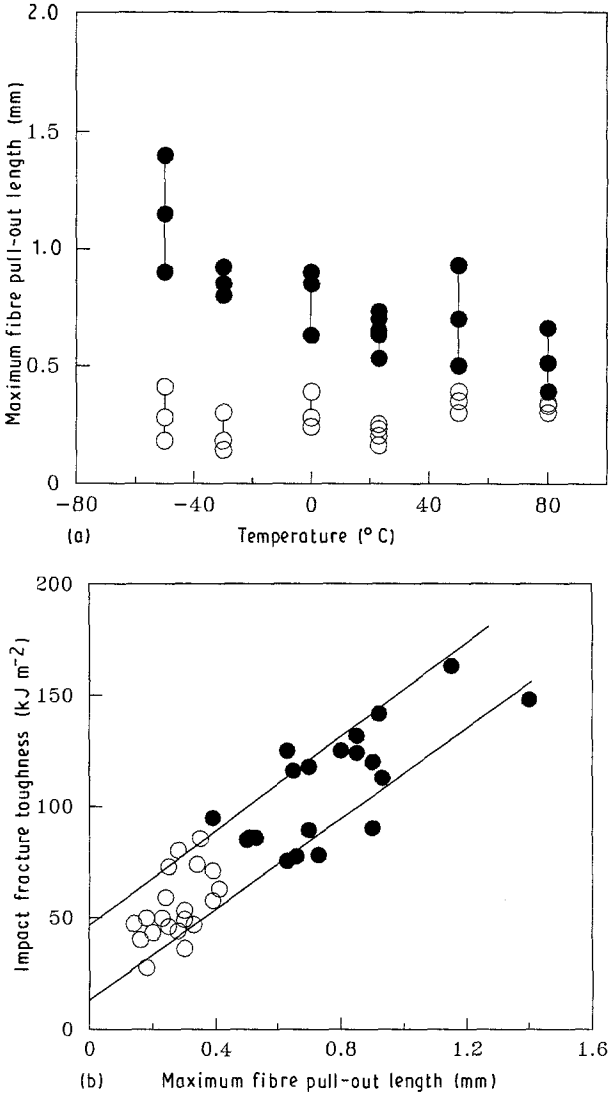

Figure 14 (a) Variation of maximum fibre pull-out length (l_{po}) with temperature and (b) impact fracture toughness as a function of maximum fibre pull-out length (l_{po}) for CFRP: (●) PVAL-coated; (○) uncoated fibres.

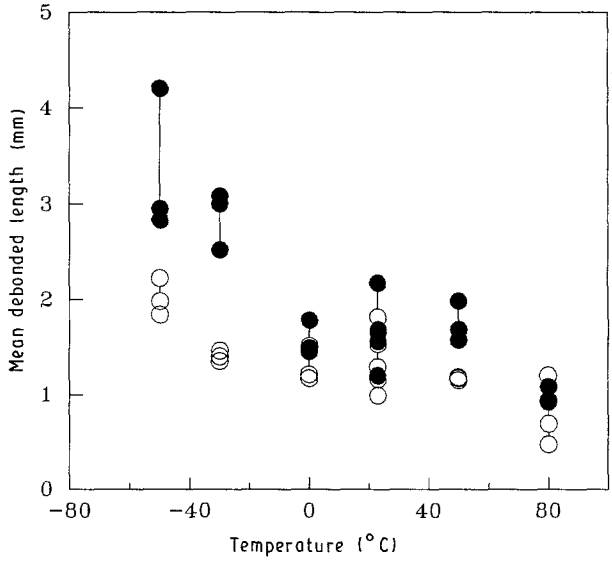

Figure 15 Variation of mean debonded length ($\bar{l}_d$) with temperature for CFRP: (●) PVAL-coated; (○) uncoated fibres.

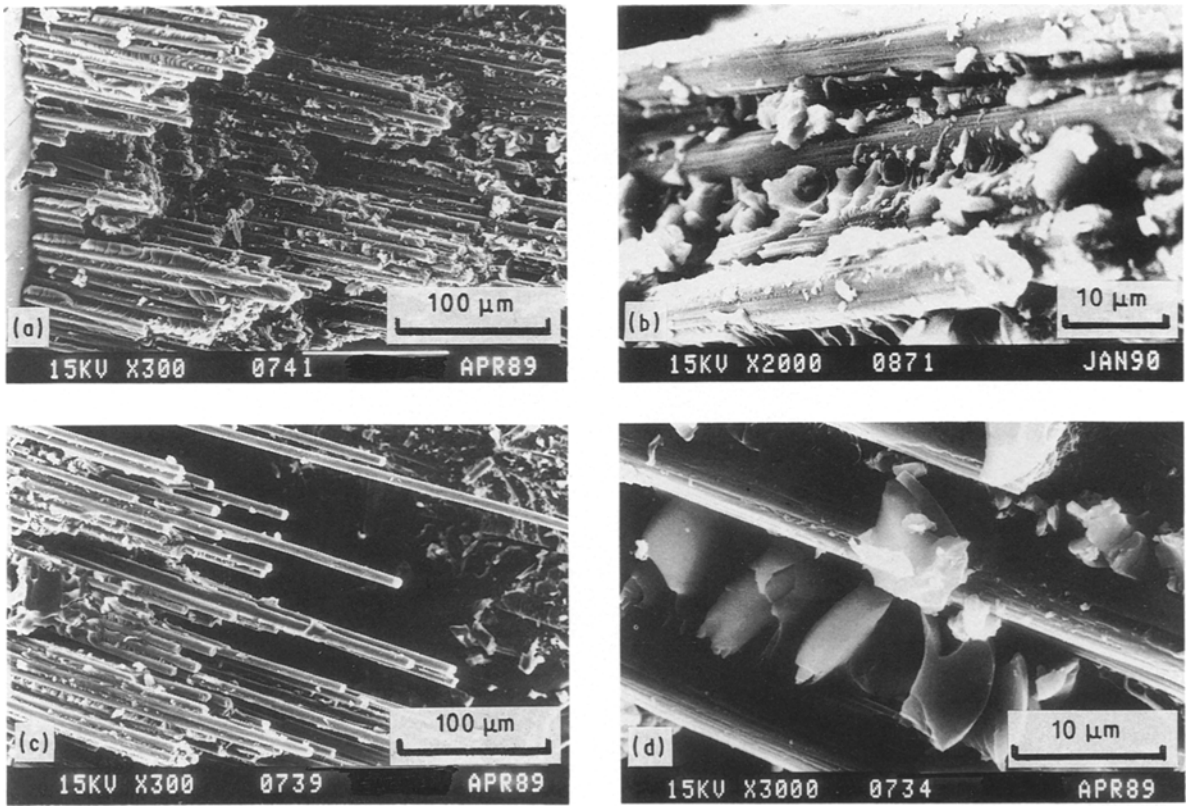

Figure 16 SEM photographs of impact fracture surfaces for CFRP: (a, b) uncoated fibres at − 30 and + 23 °C, respectively; (c, d) PVAL-coated fibres at − 50 and + 23 °C, respectively.

matrix between neighbouring fibres of pulled-out fibre bundles for both uncoated and PVAL-coated CFRP (Fig. 16b and d) are evidence of plastic deformation in the matrix material. The plastic shear may provide some toughness contribution. Single-filament pull-out tests were not performed on carbon fibres because of the difficulty in preparing test specimens with these fibres of small diameter (= 7 μm).

3.3. Delamination fracture toughness

The specific works of fracture (G_{I-II}) measured in mixed mode I–II delamination of uncoated and PVAL-coated specimens are shown in Figs 17 and 18 for KFRP and CFRP, respectively. G_{I-II} increases almost linearly with crack extension, regardless of the type of fibre used and whether the fibres are coated or not. This is attributed mainly to the increase in external constraint imposed on the specimen for the loading configuration, which not only acts as a closure force against the mode I component of a delamination crack but also facilitates a large friction between fracture surfaces. This effect is manifested by the rapid increase in G_{I-II} values near the loading points (i.e. at the end of the data points for large crack extension) where crack propagation is decelerated under

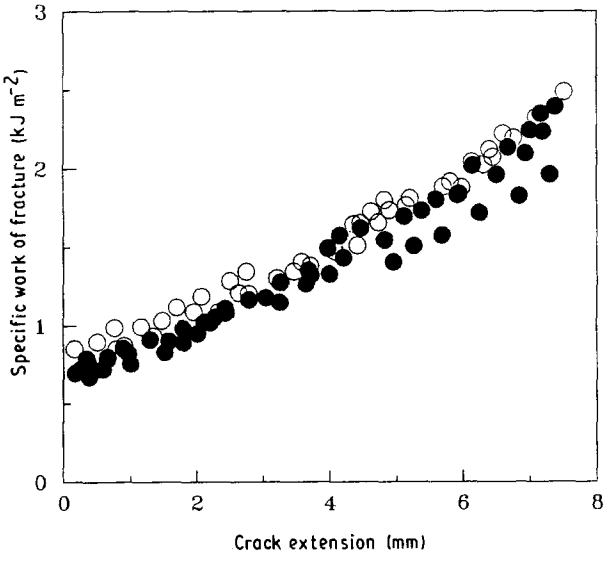

Figure 17 Specific work of fracture (G_{I-II}) for KFRP as a function of crack extension: (●) PVAL-coated; (○) uncoated fibres.

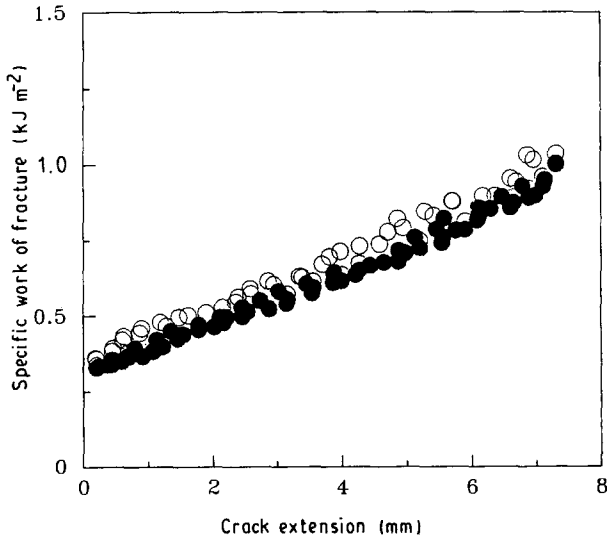

Figure 18 Specific work of fracture (G_{I-II}) for CFRP as a function of crack extension: (●) PVAL-coated; (○) uncoated fibres.

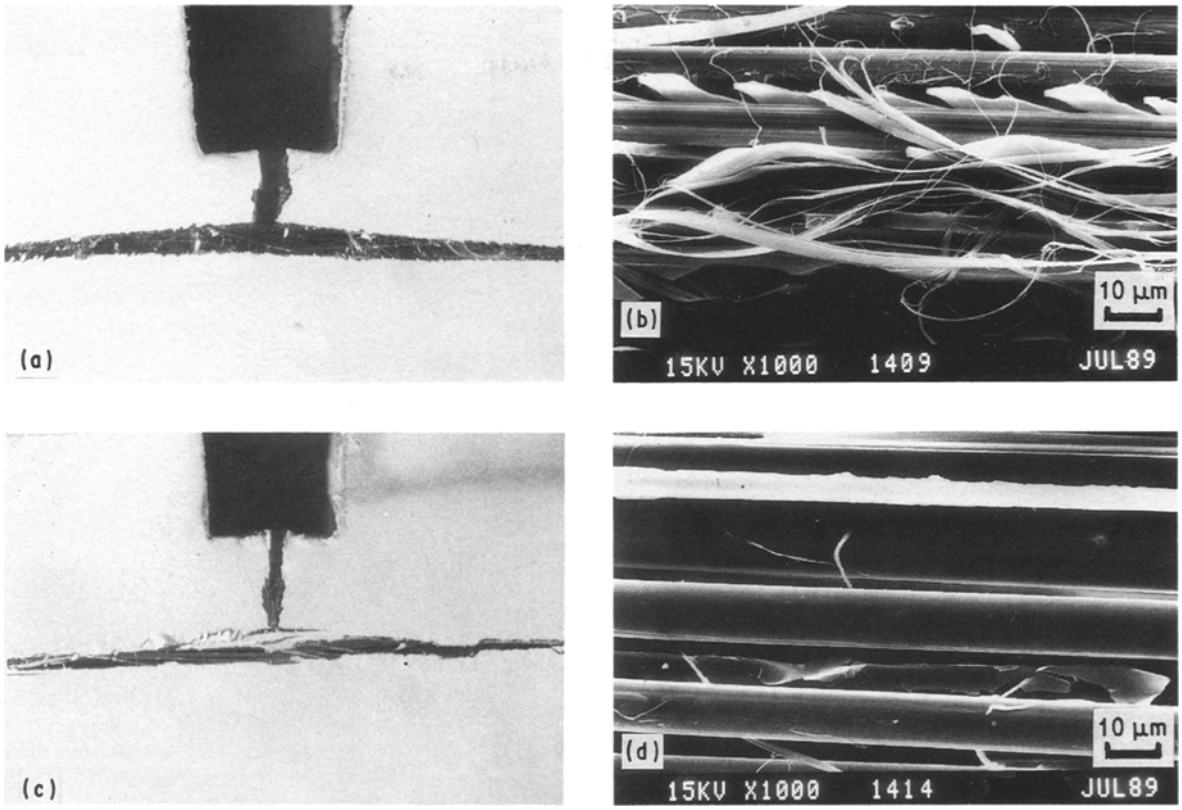

Figure 19 (a, c) Optical stereomicroscope and (b, d) SEM photographs of delamination fracture surfaces for KFRP: (a, b) uncoated fibres; (c, d) PVAL-coated fibres. (Magnification for (a) and (c) = × 20).

compression. The mode II dominant fracture loading may also have promoted additional fibre bridging, although an almost fully saturated fibre bridging zone has already been established when the very long initial delamination crack is introduced. Comparing the G_{I-II} values at a given crack extension in Figs 17 and 18, it is noted that for both KFRP and CFRP with PVAL coating they are only slightly lower (about 15%) than for the uncoated composites. This indicates that the beneficial effect of fibre coating with PVAL on the transverse fracture toughness of these composites causes little loss in the delamination fracture toughness.

In the light of the microscopic observations described below, major fracture mechanisms can be identified for the mixed-mode delamination of these composites. They are interfacial debonding, matrix deformation, fibre fracture, fibre bridging in mode I delamination [51, 52], and frictional sliding in addition to the above mechanisms in mode II delamination. Uncoated KFRP can be characterized by a single planar delamination with significant fibre bridging in the wake of the crack tip (i.e. in the tied zone) (Fig. 19a). The uncoated fibres normally split into a number of small fibrils (Fig. 19b) as observed from the fracture surfaces of transverse impact specimens. The ductile Kevlar fibre tends to facilitate bridging across the fracture surfaces over extensive lengths without being broken transversely. In contrast, PVAL-coated KFRP shows multi-planar delamination (Fig. 19c) with extensive debonding rather than fibrillation (Fig. 19d), due to their relatively low interfacial bond strength compared to the uncoated counterpart. The multi-planar delamination effectively promotes fibre bridging over several layers of fibre. It can therefore be said that for KFRP, debonding and fibre bridging are the dominant delamination fracture mechanisms while matrix fracture may be a minor one.

Delamination occurs principally in a single plane for uncoated CFRP (Fig. 20a) but is multi-planar for PVAL-coated CFRP (Fig. 20b), otherwise the fracture surfaces of both composites are similar. The existence of many broken fibres (Fig. 20c), a reflection of the brittle nature of the carbon fibre, implies that only limited fibre bridging has taken place during crack propagation. Thin epoxy layers adhering to the fibre surface, particularly in uncoated composites (Fig. 20d), are evidence of good interfacial bonding. This does not allow large debonding and fibre bridging unless there is significant misalignment of fibres across the main crack plane. Hackle markings with preferred orientation are pronounced, similar to those observed in the transverse impact specimens, suggesting that extensive shear yielding has occurred in the matrix material [53, 54]. This is partly due to strong interfacial bonding and the high modulus of carbon fibres, which force the matrix to sustain most of the deformation. A number of tiny broken epoxy particles seems to be a result of frictional sliding between rough fracture surfaces with matrix hackle markings. In summary, the primary delamination fracture mechanisms for CFRP are matrix deformation and, to a lesser extent, fibre fracture. Frictional sliding may also contribute to the delamination toughness.

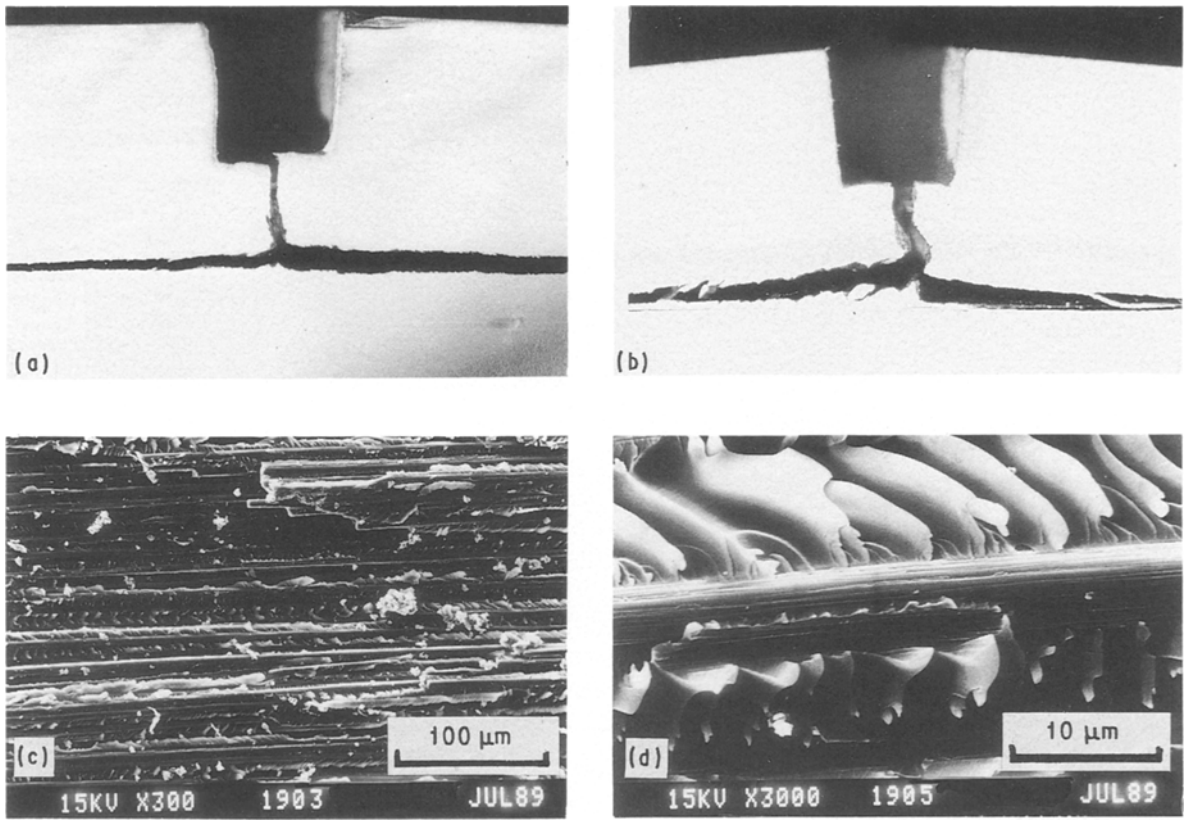

Figure 20 (a, b) Optical stereomicroscope and (c, d) SEM photographs of delamination fracture surfaces for CFRP: (a, c, d) uncoated fibres; (b) PVAL-coated fibres. (Magnification for (a) and (b) = × 20).

4. Discussion and analysis

4.1. Effect of interfacial coating

4.1.1. CTBN rubber coating

CTBN rubber has been used extensively as an additive to improve the fracture toughness of epoxy resin [55]. Although the rubber-modified epoxy increases the toughness of bulk epoxy by more than 10 times, the same increase is not obtained when the modified epoxy is used as a matrix in fibre composites. It increases the mode I delamination toughness of unidirectional CFRP by only about 75% [56]. This is attributed to the suppression of the toughening effect in a thin epoxy film between reinforcing fibres which constrains crack tip deformation. However, when the rubber-modified epoxy is reinforced with woven cloth carbon fibres, the increase can be as large as 7 times because of the presence of resin-rich regions at the strand cross-over where full deformation of the tough matrix is possible [57]. When the CTBN is used as a coating on Kevlar fibres with 3% coating concentration, the impact toughness increases only marginally (by 20%) without any significant loss of ILSS (Fig. 4 and Table I). About 40% improvement in impact fracture toughness has also been reported using this coating (of coating concentration 0.5 to 2%) for unidirectional CFRP [58]. An increase in coating concentration decreases both the fracture toughness and flexural properties. The impact specimen shows a significant plastic bending in the compressive face with relatively fewer cracks propagated in the normal and transverse directions when compared to the uncoated specimen (cf. Fig. 6a and b). The foregoing results indicate that CTBN rubber applied as a fibre coating does not remain on the fibre surface but mixes partially and reacts with the epoxy resin during curing [58]. A coating concentration as low as 0.5% seems to be sufficient to obtain desired effects of modified interfacial properties, and a large amount of coating (or large content of CTBN in the matrix) only degrades the fracture toughness and strength properties of composites (except the interlaminar fracture toughness which is matrix-dominant). This conclusion is in agreement with the previous finding [57] that the transverse fracture toughness and flexural modulus of glass fibre cloth composites with 15% CTBN rubber-modified epoxy matrix are lower than those of the same composites with unmodified epoxy.

4.1.2. PVA coating

PVA coating is not very effective for improving the fracture toughness of KFRP except at 4% coating concentration. Also, it decreases both the flexural properties and ILSS substantially (Table I). Impact specimens with this coating are characterized mainly by planar delamination across the full length of the specimen without breaking the fibres (Fig. 6c). The non-uniform coating in the form of isolated patches (Fig. 21) suggests that although the ILSS of PVA-coated fibre composites is comparable to that of PVAL coating for a given coating concentration, the apparent interfacial bond strength in the PVA-coated region is negligibly small. It should be noted here that other coatings produced fairly smooth surfaces. The

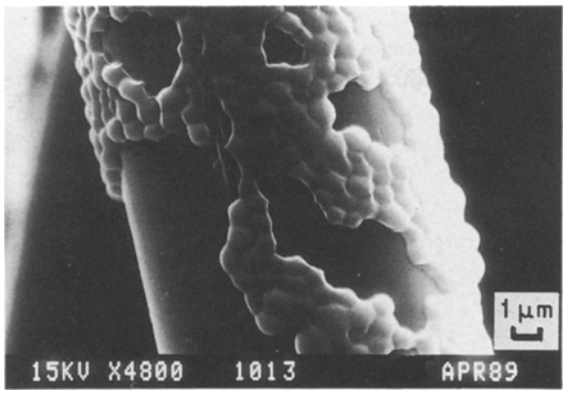

Figure 21 SEM photograph of surface morphology of a PVA-coated Kevlar fibre.

inability of cracks to propagate in the transverse direction limits the fracture process in these composites only to debonding and extensive delamination, with associated small toughness contributions.

4.1.3. PVAL coating

PVAL coating appears to be very promising in improving the fracture toughness for both KFRP and CFRP without suffering any loss in flexural strength, although slight reductions in ILSS are noted. SEM observations of the fracture surfaces of KFRP showed that uncoated fibres normally split into small fibrils in the longitudinal direction (Fig. 11b), but fibrillation is virtually absent in PVAL-coated composites (Fig. 11d). The fibrillation of the former is due probably to the skin–core heterogeneity of Kevlar fibres and the presence of inherent microvoids on the fibre surface which tend to facilitate fracture over extensive lengths to their weak outer layers [59]. The small fibrillation of PVAL-coated fibres suggests that the thermoplastic coating forms a compliant microductile layer which can satisfactorily function as (i) a stress relief medium, reducing the compressive stresses caused by thermal shrinkage of the brittle matrix [60, 61]; and (ii) a crack inhibitor or arrester facilitating large debonding in the longitudinal direction and fibre pull-out, with associated large contributions to the composite fracture toughness. The low interfacial bond strength obtained with this coating not only augments further debonding and fibre pull-out in KFRP, but it also facilitates the debonding and therefore the pulling out of individual fibres in CFRP, which otherwise fail mainly in bundles.

4.2. Effect of ligament length

It has been shown that the impact fracture toughness increases almost linearly with ligament length $(D - a)$, regardless of the type of fibre used and whether the fibres are coated or not (Figs 4 and 5). Many investigators [31, 45–47, 62] have shown a similar dependence of impact fracture toughness on $(D - a)$ for a given loading span (S). In a study of Izod impact tests of unidirectional CFRP, Hancox [45] found that the impact energy was approximately proportional to $(D - a)^2$, i.e. the toughness varied linearly with $(D - a)$, and explained this result as due to compressive failure over half the specimen depth. He suggested that compressive failure was a dominant energy-absorption mechanism. However, this explanation appeared suspect because he overestimated the strain energy absorbed in compressive failure by incorrectly assuming that the composite strength in tension and compression were equal. The high impact toughness obtained with the small span-to-depth ratio, $S/(D - a)$, is in fact related to the shear failure and other failure mechanisms induced thereby [46, 47]. The magnitude of the ratio of shear stress to normal stress developed in a beam under three-point flexure increases inversely with $S/(D - a)$. Therefore, for a given S, thin specimens (i.e. small $(D - a)$) tend to fail in flexure (either tensile fracture, compressive buckling or both), while thick specimens (i.e. large $(D - a)$) fail in shear (i.e. interfacial debonding and delamination along the fibre length) [33]. This explanation is in accord with the fracture behaviour of CFRP observed in this study, where raggedness of the fracture surface in the tension side increases with increasing $(D - a)$ (i.e. debonding and fibre pull-out are more extensive).

The same conclusion cannot be drawn for KFRP because the unbroken ligament of the specimen does not allow a similar comparison of the fracture surfaces. In addition to the direct effect of $S/(D - a)$ on the predominant failure mode, there is another factor to be considered as a result of varying the ligament $(D - a)$ for a given impact weight. If the energy applied is significantly larger than the energy necessary to fracture the ligament, the specimen tends to fail in flexure because there is little attenuation of the impact velocity [31]. In contrast, if the energy applied is only slightly larger than the energy necessary to fracture the ligament, the specimen is more likely to fail in shear by promoting debonding and/or delamination due to the large change in loading rate.

4.3. Analysis of impact fracture toughness

A general analysis for the fracture toughness of brittle-fibre reinforced brittle-matrix composites arising from various sources of failure mechanism is summarized in a review by Kim and Mai [7]. The total toughness (R_t) can be written as

$$R_t = R_s + R_{df} + R_r + R_{po} \quad (6)$$

where R_s, R_{df}, R_r and R_{po} refer to the toughness contributed by surface energy [21], post-debonding friction [2], stress redistribution [3, 4] and fibre pull-out [5, 6], respectively. R_s includes the fracture work involved in breaking the fibre (R_f) and matrix (R_m) as well as the interfacial debonding work (R_d) [1]. It should be noted, however, that it is not necessary for all these failure mechanisms to operate simultaneously for all fibre composites, and for a given composite system one or two of these toughness contributions may dominate the total fracture toughness. The validity of each failure mechanism and the corresponding toughness equation for KFRP and CFRP are described in detail as follows. To avoid any complications associated with an unbroken ligament and the

compressive failure observed in specimens made from composite laminates, failure mechanisms occurring principally in composite monolayers of sandwich specimens are discussed in this analysis.

4.3.1. Kevlar fibre composites

4.3.1.1. Surface energy. For KFRP with uncoated fibres the relatively weak interfacial bonding (compared to CFRP) does not allow large plastic deformation to occur in the matrix, and either interfacial debonding or fibrillation occurs depending on the local interfacial bond strength relative to the fibre transverse strength. For PVAL-coated KFRP, interfacial debonding occurs in preference to fibrillation. In both cases, an upper-bound estimate of debond toughness (R_d) is given by [7]

$$R_d = \frac{V_f \sigma_d^2 \bar{l}_d}{2E_f} \quad (7)$$

It is not certain as to whether tensile debonding by the Cook–Gordon mechanism [23] occurs in these composites. Judging from the observed result that the ratios of interfacial bond strength (τ_b) to matrix tensile strength (σ_m) for both uncoated and PVAL-coated specimens are greater than the required maximum strength ratio (i.e. either 1/5 for an isotropic body [23] or 1/50 for an anisotropic body [2]), this mechanism is unlikely to have occurred. Even if it had occurred under certain favourable conditions, particularly in PVAL-coated composites, the toughness contribution itself would not be significant and its ameliorating effect is represented by the increased fibre pull-out length. Therefore, a separate toughness term for the tensile debonding is not considered in this analysis.

There is some doubt on the significance of energy absorption by the Kevlar fibre fracture, although it has been included in a previous study [27] as

$$R_f = V_f \sigma_f \varepsilon_f l_g / 2 \quad (8)$$

where l_g is the gauge length at which the fibre is subjected to tension until fracture. l_g is regarded as being equal to $\bar{l}_d$ on both sides of the fracture surface, which is four times the average fibre pull-out length $\bar{l}_{po}$. Clearly, the effective l_g which determines the magnitude of R_f depends greatly on the loading condition for a given composite. Under high-velocity impact it is likely that fibre fracture occurs almost at the same time as interfacial debonding does. This implies that the usual assumption of complete fibre relaxation upon debonding is not possible, and the effective l_g during fibre deformation to fracture is significantly smaller than $\bar{l}_d$ and approximately equal to twice the fibre diameter ($d = 11.7$ μm for Kevlar 49 fibre) [63]. Therefore a lower-bound estimate of R_f can be given by

$$R_f \approx V_f \sigma_f \varepsilon_f d \quad (9)$$

Hence, the total fracture work due to the creation of new surfaces, including interfacial debonding and fibre and matrix fractures, now becomes

$$R_s = \frac{V_f \sigma_d^2 \bar{l}_d}{2E_f} + V_f \sigma_f \varepsilon_f d + (1 - V_f) R_m \quad (10)$$

4.3.1.2. Post-debonding friction. The post-debonding friction toughness (R_{df}) is the work done by the relative movement between fibre and matrix immediately after interfacial debonding as crack opening continues. An upper-bound estimate for this toughness is equal to the frictional shear force times the relative displacement between fibre and matrix. Kelly [2] suggested that this displacement is roughly the product of the debonded length ($\bar{l}_d$) and the differential strain $\Delta\varepsilon$ ($= \varepsilon_f - \varepsilon_m$). Many investigators [37, 38, 64, 65] have shown that this mechanism is one of major energy absorption mechanisms for glass fibre reinforced thermoset matrix composites. Since the frictional work is done principally by the relaxation of the cracked matrix relative to the highly stressed unbroken fibres, the differential strain $\Delta\varepsilon$ is likely to be purely elastic and any previous plastic deformation does not contribute to the relative displacement. Therefore, $\Delta\varepsilon \approx 0.01$ proposed previously [64] is considered to be a reasonable approximation. Further, since the material at both ends of the fibre remains fixed during frictional movement, the frictional work operates locally near the main fracture plane rather than over the full debond length. As suggested by Munro and Lai [38], the displacement has been modified so that the frictional work over the length near the fixed fibre ends, which is roughly the same as the fibre pull-out length (l_{po}), can be separated. Therefore, R_{df} is given as

$$R_{df} = \frac{2V_f \tau_f (\bar{l}_d - l_{po})^2 \Delta\varepsilon}{d} \quad (11)$$

4.3.1.3. Stress redistribution. The toughness due to stress redistribution is the strain energy lost by the fibre as the fibre instantly relaxes back and regains its original diameter in the matrix socket immediately after fibre fracture. This toughness term was originally proposed [3] as a sum of the work done by post-debonding friction and fibre fracture at the breaking point of the fibre, with the assumptions that the elastic transfer near the main fracture plane is small and the fibres in the region remote from the crack are unstressed. These assumptions can be satisfactorily justified under impact conditions where matrix cracking, interfacial debonding, post-debonding friction and fibre fracture occur almost at the same time, and the last two failure mechanisms operate locally near the fracture plane. Therefore, addition of this toughness term to the total toughness results in double counting.

4.3.1.4. Fibre pull-out. The fibre pull-out mechanism has been shown to be a major contributor to the fracture toughness of many types of fibre composite. The toughness equation proposed by Cottrell [5] and by Kelly and Tyson [6] is the work done by the constant friction shear stress (τ_f) over an average pull-out distance ($\bar{l}_{po}$):

$$R_{po} = \frac{2V_f \tau_f \bar{l}_{po}^2}{d} \quad (12)$$

Theoretical prediction of R_{po} using the experimental l_{po} measurement is overestimated because l_{po} is the

upper-bound maximum value measured along the profile of the projected image of pull-out fibres. The variation of pull-out length across the thickness of the composite could not be accounted for with this method. Further, the pulled-out fibres are mostly in bundles near the main fracture plane. Consequently, the overall fibre surface areas actually involved in frictional sliding are significantly smaller. Therefore, the average fibre pull-out length $\bar{l}_{po}$ is taken to be approximately one-quarter of the measured maximum l_{po} value in the calculations for R_{po}. τ_f values measured at room temperature are used for all temperatures in the absence of single-filament pull-out results at other temperatures.

The total fracture toughness (R_T) for KFRP is given by the sum of the toughness components of Equations 10 to 12.

4.3.2. Carbon fibre composites

4.3.2.1. Fibre pull-out. The fibre pull-out work (R_{po}) has been shown to be a predominant component of the fracture toughness of CFRP [10, 37, 38]. Since the interfacial properties of this composite are not available, an upper-bound estimate for R_{po} is made by assuming $l_c = 4\bar{l}_{po}$ in the usual toughness equation:

$$R_{po} = \frac{V_f \sigma_f l_c}{12} = \frac{V_f \sigma_f \bar{l}_{po}}{3} \quad (13)$$

The small variations in the tensile strength of carbon fibres (σ_f) with temperature are not included in the calculation of this toughness term.

4.3.2.2. Matrix plastic deformation. Another source of fracture toughness in CFRP is the plastic deformation of the matrix in shear. The validity of this mechanism is demonstrated by the many hackle markings which are observed on pulled-out fibre bundles (Fig. 16b and d). Plastic deformation is promoted by strong interfacial bonding and by fibres with a high stiffness and transverse strength. When the composite is subjected to axial tension, fibres with strong interfacial bonding force the matrix material in between to sustain most of the deformation along the fibre direction, until cracks developed at locally weak spots are sufficient to separate the composite into bundles of fibres. In Kevlar fibre composites where the interfacial bond strength is lower than the matrix strength, debonding occurs in preference to matrix deformation.

The energy absorbed as a consequence will be equal to the work done (U_{ms}) per unit volume in deforming the matrix to its tensile strength, multiplied by the effective volume of matrix material (V_{ms}) actually involved in plastic deformation [63, 66]. Assuming that the fibre bundles are circular in shape, V_{ms} can be estimated as the product of the matrix surface area in fibre bundles over the debond length ($\bar{l}_d$) and the depth (d_{ms}) of the deformed matrix material:

$$V_{ms} \approx n(1 - V_f)(2\pi r_b)\bar{l}_d d_{ms} \quad (14)$$

where n and r_b are the number and effective radius of the fibre bundle. Wells and Beaumont [50] estimated r_b to be 0.2 mm for a similar carbon–epoxy resin system, assuming that the bundles are about 0.5 mm wide and of thickness equal to that of one composite ply. However, it is generally observed in this study that there are tens of small bundles across the ply thickness, each bundle consisting of fibres of a similar height. Other investigators [43] reported a fibre bundle to have a few dozens of fibres. Therefore, r_b is estimated to be about 10 to 15 times the single fibre radius (i.e. $r_b \approx 0.04$ mm). The depth d_{ms} is taken approximately equal to one fibre diameter ($d = 7$ μm) as suggested previously [52, 63]. The work done per unit volume (U_{ms}) can be approximated by the product of fracture strength (σ_m) and fracture strain (ε_m) of pure epoxy resin, as determined in a tensile test. However, the epoxy resin in composites is under severe constraint due to the presence of fibres, particularly if high-stiffness fibres (e.g. carbon fibres) are involved, and under these conditions the effective stress in the matrix approaches the maximum value of about three times the measured σ_m [52]. Furthermore, hackle markings of the matrix suggest that the actual fracture strain is likely to be even higher than that obtained from the unconstrained condition. Taking into consideration the foregoing, an upper-bound estimate for U_{ms} is made as $U_{ms} \approx 3\sigma_m\varepsilon_m$. Therefore, the specific fracture energy (R_{ms}) due to matrix deformation per unit transverse cross-sectional area of the composite ($n\pi r_b^2$) is given by

$$R_{ms} \approx 6(1 - V_f)d\bar{l}_d\sigma_m\varepsilon_m/r_b. \quad (15)$$

The total toughness (R_T) for CFRP is given by the sum of the toughness components of Equations 13 and 15.

4.3.3. Comparisons of measured and predicted impact fracture toughness values

The total fracture toughness values (R_T) predicted using the equations described above and relevant data in Table II are compared with the experimental results (R_c) in Figs 22 and 23 for KFRP and CFRP, respectively. For simplicity, average values are plotted against the test temperature and standard deviations are omitted. In general, there is better agreement for CFRP than for KFRP both in magnitude and trend with temperature.

4.3.3.1. KFRP. Fig. 22a and b show that predicted R_T values are slightly lower than the experimental measurements (R_c) at all temperatures for the uncoated composites and vice versa for the PVAL-coated composites. This is associated with the difficulties in predicting accurately the post-debonding friction toughness component (R_{df}). Estimation of the relative displacement, necessary for the calculation of R_{df}, is difficult for high-velocity impact situations. However, there is no doubt that the relative displacement can be a function of debond length. There are also uncertainties in the exact values of $\bar{l}_d$ and $\bar{l}_{po}$

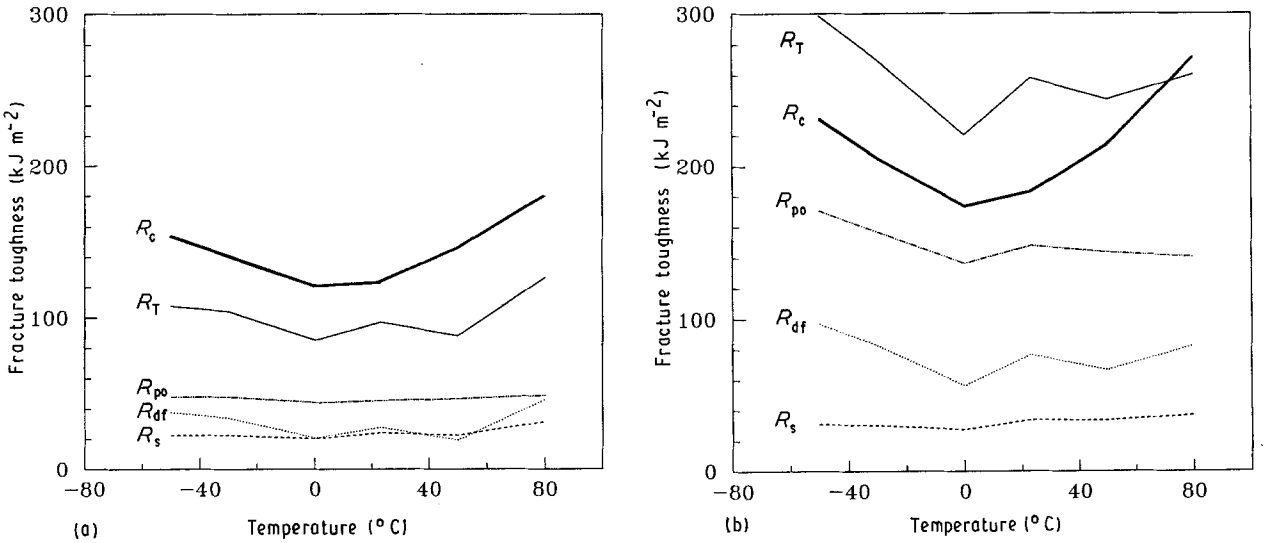

Figure 22 Comparison of predicted (R_T) and experimental (R_c) fracture toughness values for KFRP: (a) uncoated fibres; (b) PVAL-coated fibres.

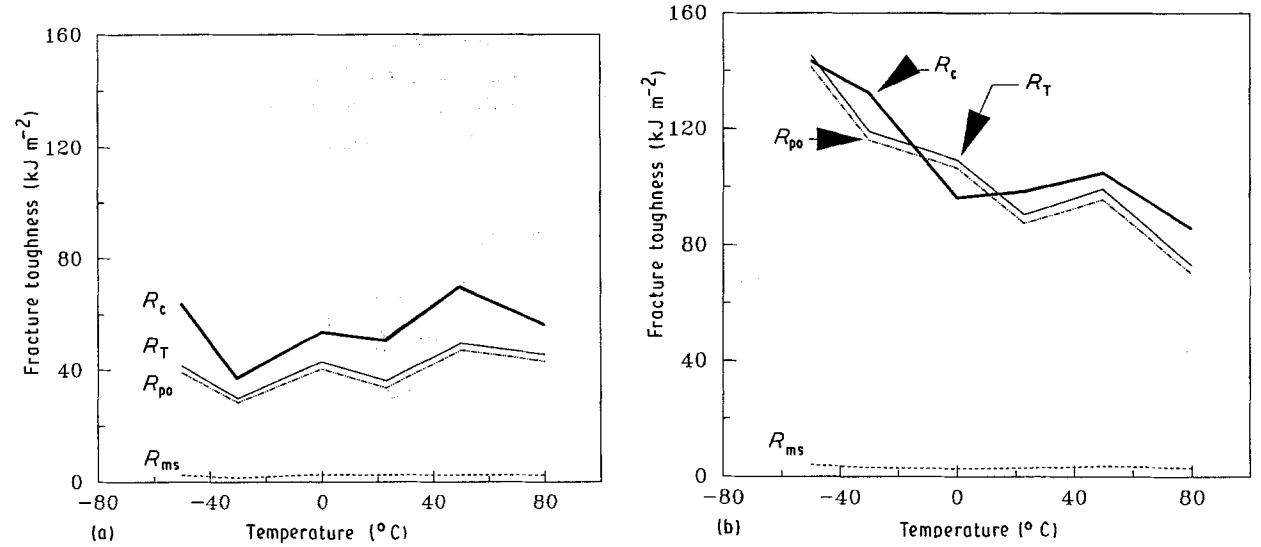

Figure 23 Comparison of predicted (R_T) and experimental (R_c) fracture toughness values for CFRP: (a) uncoated fibres; (b) PVAL-coated fibres.

which are used in the calculation of toughness components. Measurement of these values using the projected images of fracture surfaces cannot account for the variations across the thickness of the composite, as mentioned before. Nevertheless, the trends of the temperature-dependent total impact fracture toughness are well predicted both for uncoated and PVAL-coated composites.

The large increases in R_c for the coated composites at both low and high temperatures (e.g. at -50 and $+80\,^{\circ}C$) are attributed to large contributions from both fibre pull-out (R_{po}) and post-debonding friction (R_{df}). The higher fibre tensile strength (σ_f) at sub-zero temperatures (Table II) seems to be partly responsible for the improved toughness at the low temperature. Both R_{po} and R_{df} are dependent on σ_f. For a given τ_b, a high σ_f means a large critical fibre transfer length (l_c) and hence large $\bar{l}_d$ and l_{po} at low temperatures as shown in Figs 9 and 10. Judging from the similar trends in $\bar{l}_d$ for uncoated and PVAL-coated composites at temperatures higher than ambient temperature (Fig. 9), the increase in $\bar{l}_d$ at these temperatures may be associated with the temperature-dependent mechanical properties of the fibre and matrix material rather than those of the coating. The tensile strain of the matrix increases more than five times as the temperature is increased from ambient temperature to 80 °C (Table II). With reference to Fig. 22a and b it is shown that R_{po} contributes approximately 60% to the total toughness (R_T), the contribution being larger for PVAL-coated than for uncoated composites, whereas R_{df} contributes only 20 to 40% to R_T, depending on the test temperature. The increased R_{po} due to the PVAL coating is always greater than R_{df}. The surface energy R_s (which is dominated by the debond toughness, R_d) remains almost constant for all temperatures and the effect of PVAL coating is negligible.

4.3.3.2. CFRP. Very good agreement in magnitude and trend at all temperatures is obtained between

predictions and experiments for CFRP, particularly those with PVAL coating, as shown in Fig. 23a and b. The R_{po} component contributes more than 90% to the total toughness (R_T) for both composites, confirming that fibre pull-out is a dominant source of fracture toughness for this composite. R_{po} for PVAL-coated composites increases significantly as temperature is decreased, which is a direct result of the large increase in l_{po} at sub-zero temperatures (Fig. 14a). The mechanical properties of the fibre and the interfacial properties at different temperatures have not been determined, but from the observation that there are many individual fibres at the top end of the pulled-out fibre bundles, particularly at sub-zero temperatures, it can be concluded that τ_b of the coated fibre must be decreased significantly at these low temperatures. However, the physical reasons for this are not known.

It is noted that the predicted R_T is slightly lower than R_c at all temperatures for uncoated composites. This seems partly due to the somewhat underestimated contribution of the plastic shearing work of the matrix (R_{ms}). It is assumed in the analysis that fibre bundles are circular in shape. However, in reality the pulled-out fibre bundles are always of irregular shape and there are many steps along the fibre direction in a bundle. This implies that the surface area actually involved in matrix shear deformation could have been at least several times larger than that estimated on circular-shaped fibre bundles. This could result in a several times increase in R_{ms} and give better agreement between R_T and R_c for uncoated CFRP. The same argument cannot be extended to the PVAL-coated composites because the numerous debonded and pulled-out individual fibres would reduce the surface area for matrix shear plastic deformation.

5. Conclusion

The enhancement of transverse fracture toughness of continuous KFRP and CFRP has been studied using polymer coatings on the fibres. There is a substantial improvement in the impact fracture toughness of both KFRP and CFRP with PVAL coating, the improvement being by about 100%, without any loss of flexural strength. The low interfacial bond strength obtained with the PVAL coating not only augments the interfacial debonding and fibre pull-out mechanisms but also the coating eliminates fibrillation in KFRP. This indicates that the PVAL coating forms a compliant micro-ductile layer which acts as a stress relief medium and crack arrester. The large increase in toughness at low ($-50\,^{\circ}C$) and at elevated ($80\,^{\circ}C$) temperatures for PVAL-coated KFRP is mainly due to the large contributions from fibre pull-out and post-debonding friction, the former being a dominant source of total fracture toughness. The improvement in toughness for PVAL-coated CFRP is attributed largely to the pull-out of long individual fibres, particularly at sub-zero ($-50\,^{\circ}C$) temperatures, otherwise the pulled-out fibres for uncoated CFRP are principally in bundles. KFRP with PVA- or CTBN-coated fibres showed only a moderate improvement (about 20%) in toughness with 10 to 30% decrease in flexural strength for the coating concentration used. The specific work of fracture in mixed mode I–II delamination for both KFRP and CFRP with PVAL coating was slightly lower (about 15%) than for the uncoated controls. This proves that the beneficial effect of fibre coating with PVAL on transverse fracture toughness is retained in delamination fracture, and that there is little loss of damage tolerance of the composites.

Acknowledgements

The authors wish to thank the Australian Research Council (ARC) for the financial support of this work, which is part of a larger project on "Development of high strength and high toughness composites with controlled interfaces". The use of facilities at the Electron Microscopic Unit of the University of Sydney is much appreciated and thanks are also due to Dr B. Cotterell for many useful suggestions and stimulating discussions. One of us (J.K.K.) is supported by an Australian Postgraduate Research Award, a Peter Nicol Russell Postgraduate Scholarship and a Junior Research Fellowship funded by the ARC.

References

1. J. O. OUTWATER and M. C. MURPHY, in Proceedings of 24th SPI Conference, New York, 1969 (Society of Plastic Industries, 1969) Paper 11C.
2. A. KELLY, *Proc. R. Soc.* **A319** (1970) 95.
3. M. R. PIGGOTT, *J. Mater. Sci.* **5** (1970) 669.
4. J. FITZ-RANDOLPH, D. C. PHILLIPS, P. W. R. BEAUMONT and A. S. TETELMAN, *ibid.* **7** (1972) 289.
5. A. H. COTTRELL, *Proc. R. Soc.* **A282** (1964) 2.
6. A. KELLY and W. R. TYSON, *J Mech. Phys. Solids* **13** (1965) 329.
7. J. K. KIM and Y. W. MAI, *Compos. Sci. Technol.* **41** (1991).
8. B. HARRIS, P. W. R. BEAUMONT and E. MONCUNILL de FERRAN, *J. Mater. Sci.* **6** (1971) 238.
9. P. W. R. BEAUMONT and D. C. PHILLIPS, *ibid.* **7** (1972) 682.
10. P. W. R. BEAUMONT and B. HARRIS, *ibid.* **7** (1972) 1265.
11. N. L. HANCOX and H. WELLS, *Fibre Sci. Technol.* **10** (1977) 9.
12. N. H. SUNG, T. J. JONES and N. P. SUH, *J. Mater. Sci.* **12** (1977) 239.
13. J. H. WILLIAMS and P. N. KOUSIOUNELOS, *Fibre Sci. Technol.* **11** (1978) 83.
14. D. G. PEIFFER and L. E. NIELSEN, *J. Appl. Polym. Sci.* **23** (1979) 2253.
15. D. G. PEIFFER, *ibid.* **24** (1979) 1451.
16. R. V. SUBRAMANIAN and A. S. CRASTO, *Polym. Compos.* **7** (1986) 201.
17. A. S. CRASTO, S. H. OWN and R. V. SUBRAMANIAN, *ibid.* **9** (1988) 78.
18. J. P. BELL, J. CHANG, H. W. RHEE and R. JOSEPH, *ibid.* **8** (1987) 46.
19. J. CHANG, J. P. BELL and S. SHLOLNIK, *J. Appl. Polym. Sci.* **34** (1987) 2105.
20. A. S. WIMOLKIATISAK and J. P. BELL, *Polym. Compos.* **10** (1989) 162.
21. T. U. MARSTON, A. G. ATKINS and D. K. FELBECK, *J. Mater. Sci.* **9** (1974) 447.
22. A. G. ATKINS, *ibid.* **10** (1975) 819.
23. J. COOK and J. E. GORDON, *Proc. R. Soc.* **A282** (1964) 508.
24. A. G. ATKINS, *Nature* **252** (1974) 116.
25. A. G. ATKINS and Y. W. MAI, *J. Mater. Sci.* **11** (1976) 2297.
26. Y. W. MAI, *J. Mater. Sci. Lett.* **2** (1983) 723.
27. Y. W. MAI and F. CASTINO, *J. Mater. Sci.* **19** (1984) 1638.

28. *Idem, J. Mater. Sci. Lett.* **4** (1985) 505.
29. Y. W. MAI, *ibid.* **7** (1988) 581.
30. C. D. ELLIS and B. HARRIS, *J. Compos. Mater.* **7** (1973) 76.
31. L. J. BROUTMAN and A. ROTEM, in "Foreign Object Impact Damage to Composites", ASTM STP-568 (American Society for Testing and Materials, Philadelphia, 1975) p. 114.
32. P. W. R. BEAUMONT, P. G. RIEWALD and C. ZWEBEN, *ibid.* p. 134.
33. D. F. ADAMS, in "Composite Materials: Testing and Design (4th Conference)", ASTM STP-617 (American Society for Testing and Materials, Philadelphia, 1977) p. 409.
34. S. B. DRISCOLL, in "Instrumented Impact Testing of Plastics and Composite Materials", ASTM STP-936, edited by S. L. Kessler, G. C. Adams, S. B. Driscoll and D. R. Ireland. (American Society for Testing and Materials, Philadelphia, 1987) p. 163.
35. G. SANTHANKRISHNAN, R. KRISHNAMURTHY and S. K. MALHITRA, *J. Mech. Work. Technol.* **17** (1988) 195.
36. A. G. ATKINS and Y. W. MAI, "Elastic and Plastic Fracture" (Wiley, New York, 1985) p. 219.
37. J. N. KIRK, M. MUNRO and P. W. R. BEAUMONT, *J. Mater. Sci.* **13** (1978) 2197.
38. M. MUNRO and C. P. Z. LAI, *ibid.* **23** (1988) 3129.
39. N. J. JOHNSTON, NASA CP-2321 (NASA, Washington, D.C., 1984) p. 75.
40. K. KENDALL, *Proc. R. Soc.* **A344** (1975) 287.
41. H. C. CAO and A. G. EVANS, *Mech. Mater.* **7** (1989) 295.
42. J. K. KIM and Y. W. MAI, in Proceedings of 2nd Australia SAMPE Symposium and Exhibition, Melbourne, 1989, edited by F. Rose and R. Maeartney, p. 106.
43. L. SHIKHMANTER, I. ELDROR and B. CINA, *J. Mater. Sci.* **24** (1989) 167.
44. D. PURSLOW, *Composites* **12** (1981) 241.
45. N. L. HANCOX, *ibid.* **2** (1971) 41.
46. M. G. BADER and R. M. ELLIS, *ibid.* **5** (1974) 253.
47. M. G. BADER, J. E. BAILEY and I. BELL, *J. Phys. D: Appl. Phys.* **6** (1973) 572.
48. A. S. D. WANG, ASME Technical Paper 78-WA/AERO-1 (ASME, New York, 1978).
49. P. S. CHUA and M. R. PIGGOTT, *Compos. Sci. Technol.* **22** (1985) 107.
50. J. K. WELLS and P. W. R. BEAUMONT, *J. Mater. Sci.* **20** (1985) 1275.
51. R. A. CRICK, D. C. LEACH, P. J. MEAKIN and D. R. MOORE, *ibid.* **22** (1987) 2094.
52. P. J. HINE, B. BREW, R. A. DUCKETT and I. M. WARD, *Compos. Sci. Technol.* **33** (1989) 31.
53. T. JOHANNESSON, P. SJOBLON and R. SELDEN, *J. Mater. Sci.* **19** (1984) 1171.
54. L. B. ILCEWICZ, P. E. KEARY and J. TROSTLE, *Polym. Engng Sci.* **28** (1988) 592.
55. A. C. GARG and Y. W. MAI, *Compos. Sci. Technol.* **31** (1988) 179.
56. J. M. SCOTT and D. C. PHILLIPS, *J. Mater. Sci.* **10** (1975) 551.
57. W. D. BASCOM, J. L. BITNER, R. J. MOULTON and A. R. SIEBERT, *Composites* **11** (1980) 9.
58. J. F. GERARD, *Polym. Engng Sci.* **28** (1988) 568.
59. M. G. DOBB, in "Strong fibres", edited by E. Watt and B. V. Perov (North-Holland, Amsterdam, 1985) p. 673.
60. G. MAROM and R. G. C. ARRIDGE, *Mater. Sci. Engng* **23** (1976) 23.
61. L. K. BROUTMAN and B. D. AGARWAL, *Polym. Engng Sci.* **14** (1974) 581.
62. A. GOLOVOY and H. van OENE, *Polym. Compos.* **7** (1986) 56.
63. A. S. TETELMAN, in "Composite Materials: Testing and Design", ASTM STP-460 (American Society for Testing and Materials, Philadelphia, 1969) p. 473.
64. B. HARRIS, J. MORLEY and D. C. PHILLIPS, *J. Mater. Sci.* **10** (1975) 2050.
65. P. W. R. BEAUMONT and P. D. ANSTICE, *ibid.* **15** (1980) 2619.
66. G. A. COOPER and A. KELLY, *J. Mech. Phys. Solids* **15** (1967) 279.

Received 29 May
and accepted 30 November 1990